Estimation of Relative Kinematic Parameters of an Anchorless Network

Mishra, Anurodh; Rajan, Raj Thilak

DOI
10.1109/TSIPN.2025.3557585

Publication date
2025

Document Version
Final published version

Published in
IEEE Transactions on Signal and Information Processing over Networks

Estimation of Relative Kinematic Parameters of an Anchorless Network

Anurodh Mishra and Raj Thilak Rajan, *Senior Member, IEEE*

***Abstract*—Estimation of the relative positions of N static nodes in D-dimensional space given the pairwise distances between them is a well-studied problem in literature. However, for a network of mobile nodes, the existing solutions proposed in literature rely either on the knowledge of absolute positions of some nodes or enforce constraints on the motion of individual nodes to achieve a unique solution. In this work, we consider an anchorless environment and propose a time-varying Grammian-based data model which relates the relative positions of the mobile nodes to the pairwise distances between them. Given the data model, we propose algorithms to estimate the relative positions, velocity and other higher order derivatives, referred to as relative kinematics, associated with the network of mobile nodes. We further consider a scenario where accelerometers are on-board on all the mobile nodes, and investigate the inclusion the accelerometer measurements in the proposed model. The Cramér-Rao lower bound for the proposed data models are derived and compared with the performance of the estimators using Monte-Carlo simulations. We further compare and analyze the performance of the proposed estimators against the state-of-the-art methods, and present research directions for future work to further improve the proposed approach.**

***Index Terms*—Lyapunov-like equation, mobile nodes, multi-dimensional scaling, localization, time-varying distances.**

I. Introduction

THEproblem of estimating the position coordinates of N points, in a D-dimensional space, given the Euclidean distance matrix (EDM) has a long history in scientific literature and can be traced back to the works of [2], [3]. Analytical results on EDMs, in [4], [5], [6] made them an essential toolset to solve this problem, with applications in biology [7], machine learning problems [7] and signal processing [6], [8], [9], [10], [11], [12].

In the aforementioned works, EDMs are considered as static snapshots of the location of a set of points or nodes in time. In numerous applications involving motion systems, such as robot swarms [13], [14], the agents, seen as nodes, are mobile and measurements of pairwise distances between these nodes are available over time. In such cases, it is useful to model this time dependency in order to understand the underlying kinematics of the nodes. Conventionally, this problem has been treated within the context of an absolute reference frame where the absolute positions of some nodes are required to be known in order to find a unique solution to the coordinate estimation problem. For applications involving mobile nodes, especially where it is either impossible or very challenging to set up a fixed inertial reference frame, this problem provides multiple challenges. This can occur in a number of real life applications such as navigation in inaccessible environments such as disaster-hit areas [15], underwater navigation [16], [17], satellite arrays in space [18], space exploration on alien surfaces [13], indoor and outdoor wireless sensor networks [19], [20]. In such situations, a relative framework for the estimation of coordinates of the mobile nodes and their associated kinematic parameters, such as relative position, velocity, acceleration, etc., is desirable. However, there has been limited work done on the time-varying aspect of EDMs. There have been a number of works on relative localization in an anchorless network [17], [21], [22], [23]. Generally, there are two types of measurements considered. These are 'self-measurements' referring to measurements about each individual node and 'inter-node measurements' referring to measurements taken in relation to other nodes in the network. The authors in [21], [22] provide a theoretical framework for relative localization with self-measurements and inter-node measurements. In [21], an in-depth theoretical analysis of relative localization for various data models, including distance measurements is provided. Given the rotational and translational ambiguity in distance measurements, the author decomposes the error into 'relative error', which depends on the 'shape' of the network and 'transformation error' which depends on the absolute error w.r.t. the true state. It is suggested to use the orthogonal Procrustes analysis to evaluate the relative error. In [22], Fisher information matrix is used to analyze performance bounds. A general framework for network localization and navigation using belief propagation algorithm over graphical models is provided in [17], [23]. In particular, [23] uses self-measurements obtained from smartphones, including but not limited to accelerometer and gyroscope measurements, and inter-node measurements such as range information based on acoustic signals and indoor map information. The authors propose a belief propagation algorithm on the graphical model using message passing algorithm. Similarly in [17], a belief propagation based dead reckoning for underwater vehicles is proposed. The authors make use of

Received 31 December 2023; revised 25 October 2024 and 10 March 2025; accepted 17 March 2025. Date of publication 8 April 2025; date of current version 29 July 2025. This work was supported in part by European Leadership Joint Undertaking (ECSEL JU) under Grant 876019 and in part by the ADACORSA Project - "Airborne Data Collection on Resilient System Architectures." An earlier version of this paper was presented in part at European Signal Processing Conference (EUSIPCO) 2022 [DOI: 10.23919/EUSIPCO55093.2022.9909750]. The associate editor coordinating the review of this article and approving it for publication was Dr. Ji Liu. *(Corresponding author: Raj Thilak Rajan.)*

The authors are with the Signal Processing Systems, Department of Microelectronics Delft University of technology Faculty of EEMCS, 2628 Delft, CD, The Netherlands (e-mail: r.t.rajan@tudelft.nl).

Digital Object Identifier 10.1109/TSIPN.2025.3557585

speed and heading measurements with intermittent corrections based on message-passing between nodes. The position is then estimated by each node via dead-reckoning and passed to neighbors as inter-node measurements. These methods are well suited for connectivity analysis and distributed implementation.

In our work, we take the pairwise distance measurements as the inter-node measurement and include an accelerometer which meets the requirement of anchor-free localization as the self-measurement. Given their low weight and cost, they are ubiquitous in applications involving mobile nodes. In past studies, accelerometers have been combined with range-based sensors in multiple studies [24], [25], [26]. However, to the best of our knowledge, their usage has either been limited to localization in an absolute setting with known anchor positions or as part of a wider array of sensors in simultaneous localization and mapping applications [25], [26], [27], [28]. Thus, a combination of accelerometers with pairwise distances in a mobile setup for anchorless localization is desirable.

A. Related Work

Using range-based sensors for relative trajectory and pose estimation has been an important research direction but the proposed approaches rely on prior information in the estimation step [25], [26], [28], [29], [30], [31]. In communication systems, [32] proposes a range-based estimation for relative velocity of a mobile node passing by another node in ad-hoc networks but, for dense networks, the proposed algorithm requires the relative velocity of at least one set of nodes to be known. Other methods either only work in static environments [33] or provide only relative position information [14]. To our knowledge, the earliest work estimating the relative kinematics, which includes relative position and relative velocity, from time-varying Euclidean distance measurements was proposed in [34], [35] and subsequently extended in [36] for relative acceleration and higher-order kinematics. The authors presented a systematic way to estimate higher-order relative kinematics for a network of mobile nodes from time-varying distance measurements, where each node has a polynomial trajectory in time. However, in [36], to uniquely estimate the relative acceleration and other higher-order kinematics, additional rigid-body constraints are required. Recently, a Grammian-based approach to recover trajectories from time-varying pairwise distances was proposed [37] by solving a rank-constrained optimization problem. However, the proposed solution does not lead to a unique trajectory. To find a unique solution, the authors introduce spectral factorization of polynomial matrices using known anchor positions. Thus, the algorithm requires known anchor positions to estimate the relative trajectories, which goes against the premise of an anchorless setting for the work presented in this article.

B. Contributions

In this paper, our aim is to estimate the relative kinematics of a network of mobile nodes given the time-varying pairwise distance measurements without any prior knowledge of anchor nodes or references in the network. The main advantage of the proposed algorithm over the state-of-the-art in [36] is that it does not require additional rigid body constraints to be solved uniquely for the relative acceleration. The contributions made in this work are briefly listed below:

- We present a novel data model for estimating the relative kinematics of a network of mobile nodes in an anchorless setting, i.e., relative position, relative velocity and higher-order kinematics, using pairwise distance measurements.
- Relative kinematic estimators based on generalized least squares are proposed based on the new data model. Unlike the current state-of-the-art in [36], the proposed estimators do not impose any rigid body constraints on the network of mobile nodes. We achieve this by building on the work of [38] on solving a pair of Lyapunov-like equations, discussed in detail later.
- The Cramér-Rao Lower Bounds (CRLBs) for the proposed data model are derived and compared against the state-of-the-art.
- We further extend our data model to include accelerometer measurements, obtained from individual mobile nodes and propose estimators based on this extended data model.

C. Layout and Notation

Layout: Section II introduces a polynomial representation of the trajectory traversed by the network of mobile nodes and prepares the groundwork for the contribution of this paper. In Section III, a Grammian-based data model is proposed to estimate the relative kinematics of the mobile network given time-varying distances. Section IV introduces the accelerometer measurements for the mobile network and extends the Grammian-based model to include these measurements. In Section V-A, lower bounds on the variance of the estimates in the form of Cramér-Rao Lower Bounds (CRLBs) are derived for the proposed data models, and Section VI provides simulations to showcase the performance of the algorithms compared to the existing state-of-the-art.

Notation: Lower case alphabets, e.g., a, represent scalars and bold lowercase letters, e.g., $\mathbf{a}$, denote a column vector. A bold uppercase letter, e.g., $\mathbf{A}$, indicates a matrix and calligraphic letters e.g., $\mathcal{A}(\cdot)$ represent matrices that are explicitly shown to be a function of a vector or another matrix. The transpose of a matrix is denoted by $\mathbf{A}^T$. Half-vectorization of a symmetric matrix $\mathbf{A}$ is denoted by $\mathrm{vech}(\mathbf{A})$, and a standard vectorization is represented by $\mathrm{vec}(\mathbf{A})$. The symbol $\otimes$ denotes a Kronecker product and $\odot$ denotes a Hadamard product. The symbol $N!$ denotes the factorial operation given by $(\prod_{n=1}^{N} n)$. A vector and matrix of real-valued entries belong to $\mathbb{R}^N$ and $\mathbb{R}^{M\times N}$, respectively. A column vector of ones with length N is denoted by $\mathbf{1}_N$, and the l_2-norm is denoted by $\|\cdot\|$. The diagonal elements of a matrix is denoted using $\mathrm{diag}(\cdot)$ and $\mathrm{blkdiag}(\cdot,\cdot)$ denotes a matrix with the arguments along the diagonal. The element in position (i,j) in a matrix $\mathbf{A}$ is denoted by $[\mathbf{A}]_{i,j}$. Given a positive semidefinite matrix, $\mathbf{G}\in\mathbb{R}^{N\times N}$, constructed using an underlying point set $\mathbf{X}\in\mathbb{R}^{D\times N}$, the point set estimate $\widehat{\mathbf{X}}$using classical Multidimensional scaling (MDS), is given by

$$\widehat{\mathbf{X}} = \boldsymbol{\mathcal{F}}_{\mathrm{mds}}\left(\mathbf{G}\right) \tag{1a}$$

$$\triangleq \arg\min_{\mathbf{X}} \left\|\mathbf{G} - \mathbf{X}^T\,\mathbf{X}\right\| \text{ s.t. } \text{rank}(\mathbf{X}) = D \tag{1b}$$

$$= \mathbf{\Lambda}^{1/2}\,\mathbf{V}^T \tag{1c}$$

where $\mathbf{\Lambda}$ is a diagonal matrix containing the first D non-zero Eigenvalues of $\mathbf{G}$, and $\mathbf{V}$ contains the corresponding Eigenvectors [39].

II. Preliminaries

In this section, we lay the foundations for the estimation of relative kinematics for a network of mobile nodes.

A. Time-Varying Relative Kinematics

Consider a system of N mobile nodes in D-dimensional Euclidean space, whose trajectory can be modeled as an Lth degree polynomial in time t, i.e.,

$$\bar{\mathbf{S}}(t) = \sum_{l=0}^{L} (l!)^{-1}\ \overline{\mathbf{Y}}_l\, t^l, \tag{2}$$

where $\bar{\mathbf{S}}(t) \in \mathbb{R}^{D\times N}$ is the polynomial trajectory as a function of time t defined in an absolute (fixed) frame of reference [36]. Each column of $\bar{\mathbf{S}}(t)$ represents the trajectory coordinates of the corresponding nodes of the mobile network. Assuming sufficiently smooth trajectories, the lth-order derivative of this polynomial is defined as $\overline{\mathbf{Y}}_l = \bar{\mathbf{S}}^{(l)}(t)|_{t=0} \in \mathbb{R}^{D\times N}$, for $l \in \{0, 1, \ldots, L\}$, which form the matrix coefficients of the trajectory polynomial presented in (2). These coefficients, $\overline{\mathbf{Y}}_l$ are referred to as the absolute kinematic parameters of the mobile network, which represent the absolute position, velocity, etc. between the mobile nodes at $t = 0$. The associated time-varying Grammian is defined as

$$\overline{\mathbf{G}}(t) \triangleq \bar{\mathbf{S}}(t)^T\,\bar{\mathbf{S}}(t). \tag{3}$$

Let the pairwise distance between nodes i and j with $i, j \in \{1, \ldots, N\}$ be denoted by $d_{ij}(t)$. The pairwise distances can be squared and stacked in matrix form to obtain the time-varying EDM, denoted by $\mathbf{D}(t) \in \mathbb{R}^{N\times N}$ with $[\mathbf{D}(t)]_{ij} = d_{ij}^2(t)$. The time-varying EDM can be written in a matrix form using the time-varying Grammian from (3) as $\mathbf{D}(t) \triangleq \mathbf{1}_N\,\text{diag}(\overline{\mathbf{G}}(t))^T - 2\,\overline{\mathbf{G}}(t) + \text{diag}(\overline{\mathbf{G}}(t))\,\mathbf{1}_N^T$. We define the value of a time-varying function at time t_k by using the subscript k. To this end, the position coordinates at time t_k is given as

$$\overline{\mathbf{X}}_k \triangleq \bar{\mathbf{S}}(t)\Big|_{t=t_k} = \sum_{l=0}^{L} (l!)^{-1}\ \overline{\mathbf{Y}}_l\, t_k^l. \tag{4}$$

The associated EDM and Grammian matrices are given by $\mathbf{D}_k \in \mathbb{R}^{N\times N}$ and $\overline{\mathbf{G}}_k \in \mathbb{R}^{N\times N}$ respectively.

B. EDM Invariance and Centering Matrices

EDMs are invariant to any rigid transformation in the position of the underlying node network, i.e. rotations, translations and reflections. This results in infinite configurations of the mobile nodes associated with the same EDM. To get rid of the ambiguity in translation, we define the positions of the nodes in the network w.r.t. a common reference point within the network. A meaningful choice for this common reference point is the geometric centroid of the mobile network [36]. To this end, using the centering matrix, $\mathbf{C} \triangleq \mathbf{I}_N - \frac{\mathbf{1}_N\,\mathbf{1}_N^T}{N}$, we modify (2) to get the time-varying polynomial trajectory w.r.t. to the geometric centroid of the network, i.e.

$$\mathbf{S}(t) = \bar{\mathbf{S}}(t)\,\mathbf{C} = \sum_{l=0}^{L} (l!)^{-1}\ \mathbf{Y}_l\, t^l, \tag{5}$$

where $\mathbf{Y}_l \triangleq \overline{\mathbf{Y}}_l\,\mathbf{C}$ for $l \in \{0, 1, \ldots, L\}$ are the coefficients of the centered polynomial trajectory. These coefficients, $\mathbf{Y}_l$ are referred to as the relative kinematic parameters of the mobile network. The centered position coordinates $\mathbf{X}_k$ at time t_k is given as

$$\mathbf{X}_k = \overline{\mathbf{X}}_k\,\mathbf{C} = \sum_{l=0}^{L} (l!)^{-1}\ \mathbf{Y}_l\, t_k^l. \tag{6}$$

where the unknown matrix coefficients $\mathbf{Y}_0,\ \mathbf{Y}_1,\ \mathbf{Y}_2, \ldots$ denote the relative position, velocity, acceleration, etc. We are now ready to describe the problem statement for the work presented in this article.

C. Problem Statement

The focus of this work is on the estimation of relative kinematic parameters in (6) and subsequently the estimation of the relative position of the nodes in a mobile network over time.

Problem Statement: Given the pairwise distances, $\mathbf{D}_k$, over time, we aim to estimate the relative kinematics, $\mathbf{Y}_l$ for $l \in \{0, 1, \ldots, L\}$ of the mobile network. We also aim to extend the proposed solutions to incorporate accelerometer measurements to improve the relative kinematics estimates.

To this end, in Section III, a data model is proposed using pairwise distances, $\mathbf{D}_k$, which subsequently yield the relative kinematics $\mathbf{Y}_l$ for $l \in \{0, 1, \ldots, L\}$. In Section IV, an accelerometer measurement model is given, which is then used to extend the proposed data model to fuse accelerometer and pairwise distance measurements, leading to improvement in the estimates of the relative kinematics. In Section V-A, the Cramér-Rao bounds are derived to quantify the performance of the proposed data model.

III. Relative Kinematics Using Pairwise Distances

In this section, we introduce the data model based on the polynomial form of centered Grammian, $\mathbf{G}_k$ in (7). The proposed data model differs from the approach in [36], where the time-varying EDMs are modeled as polynomials in time, and [37], where the time-varying Grammian is presented as a linear combination of a set of *bases* of Grammian matrices.

A. Data Model

The Grammian matrix of the centered trajectory, $\mathbf{G}_k$, can be obtained by double-centering the EDM $\mathbf{D}_k$ at time t_k, i.e.

$$-\frac{1}{2}\,\mathbf{C}\,\mathbf{D}_k\,\mathbf{C} = \left(\overline{\mathbf{X}}_k\mathbf{C}\right)^T\,\left(\overline{\mathbf{X}}_k\,\mathbf{C}\right) = \mathbf{X}_k^T\,\mathbf{X}_k = \mathbf{G}_k, \tag{7}$$

where $\mathbf{G}_k$ is the Grammian matrix for the centered position $\mathbf{X}_k$ of the mobile network. Here we have used a property of the

centering matrix, $\mathbf{C}$, i.e. $\mathbf{C}\,\mathbf{1}_N = \mathbf{0}_N$. Substituting for $\mathbf{X}_k$ from (6) in (7), the Grammian, $\mathbf{G}_k$, for the centered coordinates, can be rewritten as

$$\mathbf{G}_k = \mathbf{B}_0 + \mathbf{B}_1\, t_k + \mathbf{B}_2\, t_k^2 + \ldots + \mathbf{B}_L\, t_k^L, \tag{8}$$

where $\mathbf{B}_l, l \in \{0, 1, \ldots, L\}$ are the coefficient of the polynomial, given by

$$\mathbf{B}_l = \sum_{m=0}^{l} \left(m!\,(l-m)!\right)^{-1}\, \mathbf{Y}_m^T\, \mathbf{Y}_{l-m}. \tag{9}$$

Unlike [36], the Grammian is directly modeled as a polynomial in time in (8) as opposed to the pairwise distances. Vectorizing (8) and using the distributive property of vectorization over summation, we get

$$\mathbf{g}_k = \mathbf{b}_0 + t_k\, \mathbf{b}_1 + t_k^2\, \mathbf{b}_2 + \ldots + t_k^L\, \mathbf{b}_L, \tag{10}$$

where $\mathbf{b}_l = \mathrm{vech}(\mathbf{B}_l)$, for $l \in \{0, 1, \ldots, L\}$ and $\mathbf{g}_k = \mathrm{vech}(\mathbf{G}_k)$. In reality, the measurements $\mathbf{D}_k$ are plagued with noise, which in turn leads to noisy $\mathbf{g}_k$. Let $\check{\mathbf{g}} = \mathbf{g} + \boldsymbol{\eta}_g$ be the noisy measurement plagued by additive zero-mean Gaussian noise with covariance matrix $\boldsymbol{\Sigma}_g$, which is discussed in Appendix A. Stacking all K timestamps, in column vector $\mathbf{t}$ for $k = \{0, \ldots, K-1\}$, we get

$$\mathbf{T}\,\boldsymbol{\theta} = \check{\mathbf{g}}, \tag{11}$$

where $\mathbf{T} = \begin{bmatrix}\mathbf{1}_K \otimes \mathbf{I}_{\overline{N}}, & \mathbf{t} \otimes \mathbf{I}_{\overline{N}}, & \ldots, & \mathbf{t}^{\odot L} \otimes \mathbf{I}_{\overline{N}}\end{bmatrix}$, $\boldsymbol{\theta} = \begin{bmatrix}\mathbf{b}_0, & \mathbf{b}_1, & \ldots, & \mathbf{b}_L\end{bmatrix}^T$, $\check{\mathbf{g}} = \begin{bmatrix}\check{\mathbf{g}}_0, & \check{\mathbf{g}}_1, & \ldots, & \check{\mathbf{g}}_K\end{bmatrix}^T$ and $\overline{N} = N(N+1)/2$.

The noise covariance $\boldsymbol{\Sigma}_g$ for the half-vectorized Grammian $\mathbf{g}_k$ hetroscedastic block diagonal structure as detailed in Appendix A. Thus, a generalized least-squares formulation is proposed, given by $\min_{\boldsymbol{\theta}} \|\boldsymbol{\Sigma}_g^{-1/2}\,(\mathbf{T}\,\boldsymbol{\theta} - \check{\mathbf{g}})\|^2$ leading to a closed-form solution of the form

$$\widehat{\boldsymbol{\theta}}_{\text{BLUE}} = \left(\mathbf{T}^T\,\boldsymbol{\Sigma}_g^{-1}\,\mathbf{T}\right)^{-1}\,\mathbf{T}^T\,\boldsymbol{\Sigma}_g^{-1}\,\check{\mathbf{g}}, \tag{12}$$

which is the *Best Linear Unbiased Estimator* or BLUE for the choice of the covariance matrix. Using the estimated $\widehat{\boldsymbol{\theta}}$, an estimate of matrix $\mathbf{B}_l$ from (9) can be reconstructed.

B. Relative Kinematics

Given the estimates of $\boldsymbol{\theta}$ and consequently $\mathbf{B}_l$ in (11), we discuss the method used to estimate the relative kinematics parameters $\mathbf{Y}_l$ of the centered mobile network. Since the uncertainty in the estimates of the coefficients $\mathbf{B}_l$ becomes worse as the order of the polynomial increases, we only consider a fourth-order approximation of the Grammian polynomial and consequently a second-order approximation to the polynomial trajectories, i.e. $\mathbf{Y}_l = \mathbf{0}$ for $l \geq 3$. Expressing the coefficients $\widehat{\mathbf{B}}_l$ from (9) for $l = \{0, 1, 2, 3, 4\}$, we get

$$\widehat{\mathbf{B}}_0 = \mathbf{Y}_0^T\,\mathbf{Y}_0, \tag{13a}$$

$$\widehat{\mathbf{B}}_1 = \mathbf{Y}_0^T\,\mathbf{Y}_1 + \mathbf{Y}_1^T\,\mathbf{Y}_0, \tag{13b}$$

$$\widehat{\mathbf{B}}_2 = \frac{1}{2}\left(\mathbf{Y}_0^T\,\mathbf{Y}_2 + \mathbf{Y}_2^T\,\mathbf{Y}_0\right) + \mathbf{Y}_1^T\,\mathbf{Y}_1, \tag{13c}$$

$$\widehat{\mathbf{B}}_3 = \frac{1}{2}\left(\mathbf{Y}_1^T\,\mathbf{Y}_2 + \mathbf{Y}_2^T\,\mathbf{Y}_1\right), \tag{13d}$$

$$\widehat{\mathbf{B}}_4 = \frac{1}{4}\,\mathbf{Y}_2^T\,\mathbf{Y}_2. \tag{13e}$$

The approximation in (13) allows for the relative position and relative acceleration to be calculated using classical MDS algorithms [1], i.e.,

$$\widehat{\mathbf{Y}}_0 = \boldsymbol{\mathcal{F}}_{\text{mds}}\left(\widehat{\mathbf{B}}_0\right), \tag{14a}$$

$$\widehat{\mathbf{Y}}_2 = \boldsymbol{\mathcal{F}}_{\text{mds}}\left(4\,\widehat{\mathbf{B}}_4\right), \tag{14b}$$

where $\widehat{\mathbf{Y}}_0$ is the estimate for the centered position coordinates $\mathbf{Y}_0$ at time $t_k = 0$ and $\widehat{\mathbf{Y}}_2$ is the estimate of the centered acceleration. It should be noted that the estimation of relative position using MDS is already proposed in [36] but our approximation also allows us to estimate the relative acceleration using MDS as well. The estimates $\widehat{\mathbf{Y}}_0$ and $\widehat{\mathbf{Y}}_2$ from the MDS solution in (14) are known only up to a rotation, which we denote by $\mathbf{H}_0$ and $\mathbf{H}_2$ respectively. We assume the rotation associated with $\widehat{\mathbf{Y}}_0$ to be identity, i.e. $\mathbf{H}_0 = \mathbf{I}_D$, which leaves the unknown rotation corresponding to $\widehat{\mathbf{Y}}_2$, given by $\mathbf{H}_2$ to be estimated. Now for $l \in \{1, 3\}$ in (9), we have the following Lyapunov-like equations

$$\mathbf{B}_1 = \mathbf{Y}_0^T\,\mathbf{Y}_1 + \mathbf{Y}_1^T\,\mathbf{Y}_0, \tag{15a}$$

$$2\,\mathbf{B}_3 = \mathbf{Y}_2^T\,\mathbf{Y}_1 + \mathbf{Y}_1^T\,\mathbf{Y}_2. \tag{15b}$$

Substituting the estimates of $\mathbf{B}_l$ from (12) for $l \in \{1, 3\}$ and the estimates of $\mathbf{Y}_0$, $\mathbf{Y}_2$ from (14), we get

$$\widehat{\mathbf{B}}_1 = \widehat{\mathbf{Y}}_0^T\,\mathbf{Y}_1 + \mathbf{Y}_1^T\,\widehat{\mathbf{Y}}_0 \tag{16a}$$

$$2\,\widehat{\mathbf{B}}_3 = \widehat{\mathbf{Y}}_2^T\,\mathbf{H}_2^T\,\mathbf{Y}_1 + \mathbf{Y}_1^T\,\mathbf{H}_2\,\widehat{\mathbf{Y}}_2, \tag{16b}$$

where the unknown relative velocity $\mathbf{Y}_1$ and the unknown rotation $\mathbf{H}_2$ needs to be estimated. To this end, in the *intermezzo* given below, we look at the particular results from [38] which are then used to present our solution.

Intermezzo: The solution to the individual equations in (16), as laid out in [38], is briefly discussed here. Given a Lyapunov-like equation of the form

$$\mathbf{A}^T\,\mathbf{P} + \mathbf{P}^T\,\mathbf{A} = \mathbf{R}, \tag{17}$$

where $\mathbf{A} \in \{\widehat{\mathbf{Y}}_0, \widehat{\mathbf{Y}}_2\}$ and $\mathbf{R} \in \{\mathbf{B}_1, 2\,\mathbf{B}_3\}$ are known and $\mathbf{P} \in \{\mathbf{Y}_1, \mathbf{H}_2^T\,\mathbf{Y}_1\}$ is unknown in (16), we consider the following definitions

$$\mathbf{A} = \mathbf{U}\,\begin{bmatrix}\boldsymbol{\Lambda}, & \mathbf{0}\end{bmatrix}\,\mathbf{V}^T, \tag{18a}$$

$$\mathbf{V}^T\,\mathbf{R}\,\mathbf{V} = \begin{bmatrix}\mathbf{R}_1, & \mathbf{R}_2 \\ \mathbf{R}_2^T, & \mathbf{0}\end{bmatrix}, \tag{18b}$$

$$\mathbf{P} = \mathbf{U}\,\begin{bmatrix}\boldsymbol{\Psi}, & \boldsymbol{\Phi}\end{bmatrix}\,\mathbf{V}^T, \tag{18c}$$

where $\mathbf{U} \in \mathbb{R}^{D\times D}$ contains the left eigenvectors, $\boldsymbol{\Lambda} \in \mathbb{R}^{D\times D}$ contains the eigenvalues and $\mathbf{V}$ contains the right eigenvectors of $\mathbf{A}$. Using the result from [38], the following relations hold

$$\psi_{ii} = r_{ii}/2\,\lambda_i, \tag{19a}$$

$$\mathbf{\Phi} = \mathbf{\Lambda}^{-1}\,\mathbf{R}_2, \tag{19b}$$

where λ_i is the ith eigenvalue of $\mathbf{\Lambda}$, ψ_{ii} is the element at ith diagonal of $\mathbf{\Psi}$, which leaves only the off-diagonal elements to be estimated. We denote the unknown off-diagonal elements with $\boldsymbol{\psi}_1$ and the known diagonal elements as $\boldsymbol{\psi}_2$ in (19a) in the vector form. Vectorizing (18c),

$$\mathbf{p} \triangleq \mathrm{vec}(\mathbf{P}) = (\mathbf{V}\otimes\mathbf{U}) = \begin{bmatrix}\boldsymbol{\psi}\\ \boldsymbol{\phi}\end{bmatrix} = (\mathbf{V}\otimes\mathbf{U})\;\mathbf{\Pi}\;\begin{bmatrix}\boldsymbol{\psi}_1\\ \boldsymbol{\psi}_2\\ \boldsymbol{\phi}\end{bmatrix}, \tag{20}$$

where $\boldsymbol{\psi} \triangleq \mathrm{vec}(\mathbf{\Psi})$, $\boldsymbol{\phi} \triangleq \mathrm{vec}(\mathbf{\Phi})$ and $\mathbf{\Pi}$ is a permutation matrix that rearranges the elements of $\begin{bmatrix}\boldsymbol{\psi}^T, & \boldsymbol{\phi}^T\end{bmatrix}^T$ to get $\begin{bmatrix}\boldsymbol{\psi}_1^T, & \boldsymbol{\psi}_2^T, & \boldsymbol{\phi}^T\end{bmatrix}^T$. Taking the result from (20), for each Lyapunov-like equation in (16), we have

$$\mathbf{y}_1 = (\mathbf{V}\otimes\mathbf{U})\;\mathbf{\Pi}\;\begin{bmatrix}\boldsymbol{\psi}_1\\ \boldsymbol{\psi}_2\\ \boldsymbol{\phi}\end{bmatrix}, \tag{21a}$$

$$(\mathbf{I}\otimes\mathbf{H}_2)\;\mathbf{y}_1 = \left(\overline{\mathbf{V}}\otimes\overline{\mathbf{U}}\right)\;\mathbf{\Pi}\;\begin{bmatrix}\overline{\boldsymbol{\psi}}_1\\ \overline{\boldsymbol{\psi}}_2\\ \overline{\boldsymbol{\phi}}\end{bmatrix}, \tag{21b}$$

where $\mathbf{U}$ and $\mathbf{V}$ are left and right eigenvectors of $\widehat{\mathbf{Y}}_0$. Similarly, $\overline{\mathbf{U}}$ and $\overline{\mathbf{V}}$ are left and right eigenvectors of $\widehat{\mathbf{Y}}_2$. Here, $\begin{bmatrix}\boldsymbol{\psi}_1^T, & \boldsymbol{\psi}_2^T, & \boldsymbol{\phi}^T\end{bmatrix}^T$ represent the vectorized and permuted form of $\mathbf{\Psi}$ and $\mathbf{\Phi}$ in (18c) for (16a) and $\begin{bmatrix}\overline{\boldsymbol{\psi}}_1^T, & \overline{\boldsymbol{\psi}}_2^T, & \overline{\boldsymbol{\phi}}^T\end{bmatrix}^T$ represent the vectorized and permuted form of $\overline{\mathbf{\Psi}}$ and $\overline{\mathbf{\Phi}}$ in (18c) for (16b). Combining the equations in (21), we have

$$\begin{bmatrix}\overline{\boldsymbol{\psi}}_1\\ \overline{\boldsymbol{\psi}}_2\\ \overline{\boldsymbol{\phi}}\end{bmatrix} = \left(\overline{\mathbf{V}}^T\otimes\overline{\mathbf{U}}^T\right)\;(\mathbf{I}\otimes\mathbf{H}_2)\;(\mathbf{V}\otimes\mathbf{U})\;\begin{bmatrix}\boldsymbol{\psi}_1\\ \boldsymbol{\psi}_2\\ \boldsymbol{\phi}\end{bmatrix}. \tag{22}$$

In (22), the number of unknowns correspond to $D^2 - D$ elements in $\boldsymbol{\psi}_1$ and D^2 elements in $\mathbf{H}_2$. Observe that the number of unknowns in (22) depends only on the dimension D, i.e. $2\,D^2 - D$. However, the number of equations in (22) depends on both D and N and is given by $(N-D)D + D$. This proves useful in defining the number of nodes required to solve (22) for any dimension D. (22) is nonlinear due to the cross-terms between $\mathbf{H}_2$ and $\boldsymbol{\psi}_1$. Expanding the expressions further and ignoring the rows associated with unknown $\overline{\boldsymbol{\psi}}_1$, (22) can be rewritten as a linear basis function model of the form

$$\begin{bmatrix}\overline{\boldsymbol{\psi}}_2\\ \overline{\boldsymbol{\phi}}\end{bmatrix} = \mathbf{W}\,\boldsymbol{\xi}(\boldsymbol{\psi}_1, \mathbf{h}_2), \tag{23}$$

where $\mathbf{h}_2 \triangleq \mathrm{vec}(\mathbf{H}_2)$, $\boldsymbol{\xi}(\boldsymbol{\psi}_1, \mathbf{h}_2)$ contains the cross-terms and $\mathbf{W}$ contains the corresponding coefficients associated with the cross-terms. To estimate the unknowns $\boldsymbol{\psi}_1$ and $\mathbf{h}_2$, (23) can be posed as a least squares problem given by

$$\widehat{\boldsymbol{\psi}}_1, \widehat{\mathbf{h}}_2 = \arg\min_{\boldsymbol{\psi}_1, \mathbf{h}_2} \left\| \begin{bmatrix}\overline{\boldsymbol{\psi}}_2\\ \overline{\boldsymbol{\phi}}\end{bmatrix} - \mathbf{W}\,\boldsymbol{\xi}(\boldsymbol{\psi}_1, \mathbf{h}_2)\right\|^2. \tag{24}$$

The problem is uniquely solvable if $\mathbf{W}$ is invertible, which is true for the given case as discussed in the Appendix D. An alternate formulation exploits the known structure of $\mathbf{h}$ using the orthogonality constraint, i.e.

$$\widehat{\boldsymbol{\psi}}_1, \widehat{\mathbf{h}}_2 = \arg\min_{\boldsymbol{\psi}_1, \mathbf{h}_2} \left\| \begin{bmatrix}\overline{\boldsymbol{\psi}}_2\\ \overline{\boldsymbol{\phi}}\end{bmatrix} - \mathbf{W}\,\boldsymbol{\xi}(\boldsymbol{\psi}_1, \mathbf{h}_2)\right\|^2, \quad \text{s.t.} \quad \mathbf{H}_2^T\,\mathbf{H}_2 = \mathbf{I}_D. \tag{25}$$

Once $\widehat{\boldsymbol{\psi}}_1$ and $\widehat{\mathbf{h}}_2$ are estimated, the relative velocity, $\widehat{\mathbf{Y}}_1$, can be estimated using the relation in (21a). The details of the solvability of (23) are discussed further in detail in Appendix D. It should be noted that we have not included the information from (13c) in the estimates of $\widehat{\mathbf{Y}}_1$ and $\widehat{\mathbf{H}}_2$. To further improve the estimates, the entire optimization problem, corresponding to $\mathbf{B}_l$, $l \in \{1,2,3\}$ can be posed a constrained nonlinear least squares problem

$$\widehat{\mathbf{y}}_1,\, \widehat{\mathbf{h}}_2 = \arg\min_{\mathbf{y}_1,\,\mathbf{h}_2} \left\|\widehat{\mathbf{b}}_1 - \mathbf{C}_1\,\mathbf{y}_1\right\| + \left\|2\,\widehat{\mathbf{b}}_3 - \mathbf{C}_2\,\widetilde{\mathbf{y}}_1\right\|, \tag{26a}$$

$$\text{s.t.} \quad \mathbf{C}_3\,\mathbf{h}_2 + 2\,\mathrm{hvec}\left(\mathbf{Y}_1^T\,\mathbf{Y}_1\right) = 2\,\widehat{\mathbf{b}}_2, \tag{26b}$$

$$\widetilde{\mathbf{Y}}_1 = \mathbf{H}_2\,\mathbf{Y}_1, \tag{26c}$$

where $\mathbf{C}_1 \triangleq (\mathbf{I}\otimes\widehat{\mathbf{Y}}_0^T) + (\widehat{\mathbf{Y}}_0^T\otimes\mathbf{I})\,\mathbf{J}$, $\mathbf{C}_2 \triangleq (\mathbf{I}\otimes\widehat{\mathbf{Y}}_2^T) + (\widehat{\mathbf{Y}}_2^T\otimes\mathbf{I})\,\mathbf{J}$ and $\mathbf{C}_3 \triangleq (\widehat{\mathbf{Y}}_2^T\otimes\widehat{\mathbf{Y}}_0^T) + (\widehat{\mathbf{Y}}_0^T\otimes\widehat{\mathbf{Y}}_2^T)\,\mathbf{J}$ with $\mathbf{J}$ as the commutation matrix. The estimates of $\widehat{\mathbf{Y}}_1$ and $\widehat{\mathbf{H}}_2$ from (16) and (23) can be used as a starting point to solve (26) to potentially avoid any local minima.

In summary, the coefficients, $\mathbf{B}_l$, of the centered Grammian polynomial in (9) are estimated using (12). Using these coefficient estimates, the relative position and relative acceleration with arbitrary rotation is estimated using (14). To solve for the arbitrary rotation associated with the acceleration, $\mathbf{H}_2$ and the relative velocity $\mathbf{Y}_1$, the set of Lyapunov-like equations in (16) is solved using the scheme proposed in this section. Algorithm 1 summarizes the proposed scheme for estimating the relative kinematic parameters using only pairwise distances.

Algorithm 1: Relative Kinematics Using Pairwise Distances.

1: **Input:** Pairwise distances $\mathbf{D}_k$ for all t_k, $k \in \{0,\ldots,K\}$.
2: For all t_k, calculate $\mathbf{G}_k$ from $\mathbf{D}_k$ using (7).
3: Solve for $\widehat{\mathbf{B}}_l$ using (12).
4: Estimate $\widehat{\mathbf{Y}}_0$ and $\widehat{\mathbf{Y}}_2$ using $\widehat{\mathbf{B}}_0$ and $\widehat{\mathbf{B}}_4$ in (14).
5: Solve for $\widehat{\mathbf{Y}}_1$ and $\widehat{\mathbf{H}}_2$ using $\widehat{\mathbf{B}}_1$ and $\widehat{\mathbf{B}}_3$ in (16).
6: **Output:** $\widehat{\mathbf{Y}}_0$, $\widehat{\mathbf{Y}}_1$, $\widehat{\mathbf{Y}}_2$ and $\widehat{\mathbf{H}}_2$.

IV. Relative Kinematics Using Pairwise Distances and Accelerometers

We now consider a scenario where all the nodes have an accelerometer, and subsequently extend our existing data model to incorporate these accelerometer measurements. For the centered polynomial trajectory given in (5), the centered acceleration, $\ddot{\mathbf{X}}_k$ associated with the mobile network at time t_k, can be obtained by twice differentiating $\mathbf{S}(t)$ w.r.t. time, i.e.

$$\ddot{\mathbf{X}}_k = \frac{\partial^2 \mathbf{S}(t)}{\partial t^2}\bigg|_{t=t_k} = \sum_{l=2}^{L} \left((l-2)!\right)^{-1} \mathbf{Y}_l \, t_k^{l-2}. \tag{27}$$

In vectorized form, we have

$$\ddot{\mathbf{x}}_k = \text{vec}\left(\ddot{\mathbf{X}}_k\right) = \sum_{l=2}^{L} \left((l-2)!\right)^{-1} \mathbf{y}_l \, t_k^{l-2}. \tag{28}$$

In the previous sections, we have considered the problem of estimating the relative kinematic parameters $\mathbf{Y}_l$ using only pairwise distances and introduced a data model in Section III. With the added accelerometer per node, we look into the possibility of improving the relative kinematic estimates and discuss the underlying assumptions made. In Section IV-A, the accelerometer measurement model is introduced. In Section IV, the proposed data model from Section III is modified to include the accelerometer measurements.

A. Accelerometer Measurement Model

The accelerometer measurement model for a mobile node i for the centered trajectory at time t_k, is given by

$$\ddot{\tilde{\mathbf{x}}}_{i,k} = \mathbf{Q}_{i,k} \, \ddot{\mathbf{x}}_{i,k} + \boldsymbol{\epsilon}_{i,k}, \tag{29}$$

where $\ddot{\tilde{\mathbf{x}}}_{i,k}, \ddot{\mathbf{x}}_{i,k} \in \mathbb{R}^D$ are the noisy and true acceleration (centered at the origin) and $\mathbf{Q}_{i,k}$ is the rotation matrix associated with the accelerometer frame for node i at time t_k. The measurements are accompanied by white Gaussian noise, i.e. $\boldsymbol{\epsilon}_{i,k} \sim \mathcal{N}(0, \sigma_a^2 \, \mathbf{I}_D)$ [40, Chapter 2]. Without loss of generality, we assume a calibrated accelerometer. Stacking the accelerometer measurements for each mobile node as columns in a matrix, we have

$$\ddot{\tilde{\mathbf{X}}}_k = \begin{bmatrix} \mathbf{Q}_{1,k} \, \ddot{\mathbf{x}}_{1,k}, & \mathbf{Q}_{2,k} \, \ddot{\mathbf{x}}_{2,k}, & \ldots, & \mathbf{Q}_{N,k} \, \ddot{\mathbf{x}}_{N,k} \end{bmatrix} + \mathbf{E}_k. \tag{30}$$

Using the vectorized form of centered acceleration from (28), (30) can be vectorized as

$$\ddot{\tilde{\mathbf{x}}}_k = \sum_{l=2}^{L-2} \left((l-2)!\right)^{-1} \widetilde{\mathbf{y}}_l \, t_k^{l-2} + \boldsymbol{\epsilon}_k, \tag{31}$$

where $\ddot{\tilde{\mathbf{x}}}_k = \begin{bmatrix} \ddot{\tilde{\mathbf{x}}}_{1,k} & \ddot{\tilde{\mathbf{x}}}_{2,k}, & \ldots, \ddot{\tilde{\mathbf{x}}}_{N,k} \end{bmatrix}^T$ and $\widetilde{\mathbf{y}}_l = \mathbf{Q}_k \, \text{vec}(\mathbf{Y}_l)$ with $\mathbf{Q}_k \triangleq \text{blkdiag}(\mathbf{Q}_{1,k}, \ldots, \mathbf{Q}_{N,k})$. To model the time-varying rotations, $\mathbf{Q}_{i,k}$, for each node i, additional information is required about the relationship between rotations at different times t_k. In absence of such information, the system of equations in (31) is not useful and the number of unknowns in $\mathbf{Q}_k$ increases with each k.

Assumption: In absence of any additional measurement, we assume that $\mathbf{Q}_{i,k}$, for each node i, is constant, which implies that the accelerometer measurements are obtained w.r.t. a non-rotating frame of reference. These conditions are only applicable in situations where the mobile nodes under investigation are holonomic motion systems[42] or a transformation is available at all times that allows for the construction of $\ddot{\tilde{\mathbf{x}}}_k$ w.r.t. a common frame for all k.

Under the given assumption, two cases naturally arise:

1) Initial rotation values are constant but distinct, i.e.
$$\mathbf{Q}_k = \mathbf{Q} = \text{blkdiag}\left(\mathbf{Q}^{(1)}, \ldots, \mathbf{Q}^{(N)}\right), \tag{32}$$
with $\mathbf{Q}^{(i)} \in \mathbb{R}^{D \times D}, \forall i \in \{1, 2, \ldots, N\}$.
2) Initial rotation values are constant and identical, i.e.
$$\mathbf{Q}_k = \mathbf{Q} \otimes \mathbf{I}_N, \tag{33}$$
with $\mathbf{Q} \in \mathbb{R}^{D \times D}$ resulting in $\widetilde{\mathbf{Y}}_l = \mathbf{Q} \, \mathbf{Y}_l$.

The first case is essentially a more restrictive version of the second case. These cases imply that the mobile nodes are traversing through the D-dimensional space with fixed rotational degrees of freedom, e.g. in a drone light show [43]. To include time-varying rotation for the mobile nodes, additional sensors, e.g. gyroscope, are required, which is beyond the scope of this work. In the next subsections, we propose a least squares estimator to estimate the coefficients $\widetilde{y}_l$, $l \geq 2$ from the accelerometer measurements and discuss how these coefficients can be used for the two cases in (32) and (33) (34a)-(34d) shown at the bottom of the next page.

B. Estimates Using Accelerometer Measurements

The accelerometer measurements in (31) for K timestamps can be stacked together in a column vector given by

$$\check{\boldsymbol{\tau}} = \mathbf{V} \, \boldsymbol{\alpha}, \tag{35}$$

where $\mathbf{V} = \begin{bmatrix} \mathbf{1}_K \otimes \mathbf{I}_{ND}, & \mathbf{t_k} \otimes \mathbf{I}_{ND}, & \ldots, & \mathbf{t_k}^{\odot L-2} \otimes \mathbf{I}_{ND} \end{bmatrix}$, $\boldsymbol{\alpha} = \begin{bmatrix} \widetilde{\mathbf{y}}_2, & \widetilde{\mathbf{y}}_3, & \ldots & \widetilde{\mathbf{y}}_L \end{bmatrix}^T$, $\check{\boldsymbol{\tau}} = \begin{bmatrix} \check{\boldsymbol{\tau}}_0, & \check{\boldsymbol{\tau}}_1, & \ldots, & \check{\boldsymbol{\tau}}_K \end{bmatrix}^T$ with $\check{\boldsymbol{\tau}}_k = \ddot{\tilde{\mathbf{x}}}_k$. The closed form estimate for the accelerometer coefficients can be obtained by solving the least-squares problem $\arg\min_{\boldsymbol{\alpha}} \|\mathbf{V} \, \boldsymbol{\alpha} - \check{\boldsymbol{\tau}}\|_2^2$ leading to

$$\widehat{\boldsymbol{\alpha}} = \left(\mathbf{V}^T \, \mathbf{V}\right)^{-1} \mathbf{V}^T \, \check{\boldsymbol{\tau}}, \tag{36}$$

which is an optimal unbiased estimate of the acceleration coefficients, $\widetilde{\mathbf{y}}_l$, under the assumption of white Gaussian noise model, where $\widetilde{\mathbf{Y}}_l \triangleq \text{vech}(\widetilde{\mathbf{y}}_l)$, $\forall l = \{0, 1, \ldots, L\}$.

C. Constant and Distinct Initial Rotations

For the assumption in (32), the coefficient estimates $\widetilde{\mathbf{y}}_l$ can be used to estimate the relative orientation between the mobile nodes. To this end, consider the estimate $\widehat{\mathbf{B}}_4$ from (12). Let $[\mathbf{B}_4]_{i,j}$ denote the element at position $\{ij\}$ of the matrix and $[\mathbf{Y}_2]_i$ denote the ith column of matrix $\mathbf{Y}_2$. Thus, using (13), we have

$$4 \, [\widehat{\mathbf{B}}_4]_{ij} = [\mathbf{Y}_2]_i^T \, [\mathbf{Y}_2]_j$$

$$= [\widetilde{\mathbf{Y}}_2]_i^T \, \mathbf{Q}_i^T \, \mathbf{Q}_j \, [\widetilde{\mathbf{Y}}_2]_j$$
$$= [\widetilde{\mathbf{Y}}_2]_i^T \, \mathbf{Q}_{ij} \, [\widetilde{\mathbf{Y}}_2]_j,$$

where $\mathbf{Q}_{ij}$ is the relative orientation between nodes i and j. Thus, the relative orientation can be estimated by solving the following constrained least squares problem

$$\widehat{\mathbf{Q}}_{ij} = \arg\min_{\mathbf{Q}_{ij}} \quad \left\| 4\,[\widehat{\mathbf{B}}_4]_{ij} - [\widetilde{\mathbf{Y}}_2]_i^T \, \mathbf{Q}_{ij} \, [\widetilde{\mathbf{Y}}_2]_j \right\|^2,$$
$$\text{s.t.} \quad \mathbf{Q}_{ij}^T \, \mathbf{Q}_{ij} = \mathbf{I}_D. \tag{37}$$

For consistency between the relative rotation of the mobile nodes, we have

$$\mathbf{Q}_{ij} = \mathbf{Q}_{ik} \, \mathbf{Q}kj, \quad \forall k. \tag{38}$$

The additional constraints in (38) can be used to further constrain the solution.

D. Constant and Identical Initial Rotation

For the assumption in (33) and given $\widetilde{\mathbf{Y}}_l, l \geq 2$ estimates from (36), the formulation in (8) can be modified such that

$$\widetilde{\mathbf{G}}_k = \widetilde{\mathbf{B}}_0 + \widetilde{\mathbf{B}}_1 \, t_k + \widetilde{\mathbf{B}}_2 \, t_k^2 + \ldots + \widetilde{\mathbf{B}}_{L-1} \, t_k^{L-1}, \tag{39}$$

where $\widetilde{\mathbf{G}}_k = \mathbf{G}_k - \sum_{l=2}^{L} (l!)^{-2} \, \widetilde{\mathbf{Y}}_l^T \, \widetilde{\mathbf{Y}}_l$ and $\widetilde{\mathbf{B}}_l = \sum_{m=0;m\neq l,\forall l>2}^{l} (m!\,(l-m)!)^{-1} \, \widetilde{\mathbf{Y}}_m^T \, \widetilde{\mathbf{Y}}_{l-m}$ for $l \in \{0, 1, \ldots, L-1\}$. Here, we define $\widetilde{\mathbf{Y}}_l = \mathbf{Y}_l$ for $l \leq 1$. Vectorizing (39), we get

$$\widetilde{\mathbf{r}}_k = \widetilde{\mathbf{b}}_0 + t_k \, \widetilde{\mathbf{b}}_1 + t_k^2 \, \widetilde{\mathbf{b}}_2 + \ldots + t_k^L \, \widetilde{\mathbf{b}}_{L-1}, \tag{40}$$

where $\widetilde{\mathbf{b}}_l = \text{vech}(\widetilde{\mathbf{B}}_l)$, for $l \in \{0, 1, \ldots, L-1\}$ and $\widetilde{\mathbf{r}}_k = \text{vech}(\widetilde{\mathbf{G}}_k)$. Without loss of generality, let $\check{\mathbf{r}}_k = \widetilde{\mathbf{r}}_k + \boldsymbol{\eta}_r$ be the noisy measurement plagued by additive Gaussian noise with covariance matrix $\boldsymbol{\Sigma}_{r_k}$. Stacking all K timestamps in column vector $\check{\mathbf{r}}$, (40) can be extended as,

$$\widetilde{\mathbf{T}} \, \widetilde{\boldsymbol{\theta}} = \check{\mathbf{r}} \tag{41}$$

where $\widetilde{\mathbf{T}} = \left[\mathbf{1}_K \otimes \mathbf{I}_{\overline{N}}, \quad \mathbf{t} \otimes \mathbf{I}_{\overline{N}}, \quad \ldots, \quad \mathbf{t}^{\odot L-1} \otimes \mathbf{I}_{\overline{N}}\right]$, $\widetilde{\boldsymbol{\theta}} = \left[\widetilde{\mathbf{b}}_0, \quad \widetilde{\mathbf{b}}_1, \quad \ldots, \quad \widetilde{\mathbf{b}}_{L-1}\right]^T$ and $\check{\mathbf{r}} = \left[\check{\mathbf{r}}_0, \quad \ldots, \quad \check{\mathbf{r}}_K\right]^T$. Similar to Sections III-A, the estimation problem for $\widetilde{\boldsymbol{\theta}}$ in (41) can be posed as a generalized least squares problem given by $\arg\min_{\widetilde{\boldsymbol{\theta}}} \|\boldsymbol{\Sigma}_r^{-1/2} \, (\widetilde{\mathbf{T}} \, \widetilde{\boldsymbol{\theta}} - \check{\boldsymbol{r}})\|_2^2$ which admits a solution

$$\widehat{\widetilde{\boldsymbol{\theta}}} = \left(\widetilde{\mathbf{T}}^T \, \boldsymbol{\Sigma}_r^{-1} \, \widetilde{\mathbf{T}}\right)^{-1} \, \widetilde{\mathbf{T}}^T \, \boldsymbol{\Sigma}_r^{-1} \, \check{\mathbf{r}}. \tag{42}$$

Algorithm 2: Relative Kinematics Using Pairwise Distances and Accelerometer Measurements.

1: **Input:** Pairwise distances, $\mathbf{D}_k$, and centered accelerometer measurements, $\ddot{\widetilde{\mathbf{X}}}_k$, for all t_k, $k \in \{0, \ldots, K\}$.
2: For all t_k, calculate $\mathbf{G}_k$ from $\mathbf{D}_k$ using (7).
3: Estimate $\widetilde{\mathbf{Y}}_l$ for $l \geq 2$ using (36).
4: Solve for $\widehat{\mathbf{B}}_l$ using (42).
5: Estimate $\widehat{\mathbf{Y}}_0$ using $\widehat{\mathbf{B}}_0$ in (14a).
6: Solve for $\widehat{\mathbf{Y}}_1$ and $\widehat{\mathbf{Q}}$ using $\widehat{\mathbf{B}}_1$ and $\widehat{\mathbf{B}}_3$ in (43).
7: **Output:** $\widehat{\mathbf{Y}}_0$, $\widehat{\mathbf{Y}}_1$, $\widehat{\mathbf{Y}}_2$ and $\widehat{\mathbf{Q}}$.

E. Relative Kinematics Estimate

The relative position estimate at time $t = 0$ can be calculated by solving for $\mathbf{Y}_0$ in (14a). The estimate $\widehat{\widetilde{\mathbf{Y}}}_2$ from (36) has an unknown rotation $\mathbf{Q}$ corresponding to the non-rotating accelerometer frame that needs to be estimated. Hence, to estimate the remaining unknowns, $\mathbf{Y}_1$ and $\mathbf{Q}$, consider the following set of equations

$$\widehat{\mathbf{B}}_1 = \widehat{\mathbf{Y}}_0^T \, \mathbf{Y}_1 + \mathbf{Y}_1^T \, \widehat{\mathbf{Y}}_0, \tag{43a}$$
$$2\,\widehat{\mathbf{B}}_3 = \widehat{\widetilde{\mathbf{Y}}}_2^T \, \mathbf{Q}^T \, \mathbf{Y}_1 + \mathbf{Y}_1^T \, \mathbf{Q} \, \widehat{\widetilde{\mathbf{Y}}}_2, \tag{43b}$$

which can be solved for $\mathbf{Y}_1$ and $\mathbf{Q}$ using the solving scheme introduced in Section III-B. The proposed scheme in the presence of accelerometer measurements along with pairwise distances is summarized in Algorithm 2. It should be noted that, unlike the second-order approximation in Section III-B, given the accelerometer measurements, Algorithm 2 does not make this assumption and can be used for a general polynomial trajectory of any order L.

$$\mathbf{Y}_0 = \begin{bmatrix} -244, & 385, & 81, & -19, & -792, & -554, & -965, & -985, & -49, & -503 \\ -588, & -456, & -992, & -730, & 879, & 970, & 155, & 318, & -858, & 419 \end{bmatrix} \tag{34a}$$

$$\overline{\mathbf{Y}}_1 = \begin{bmatrix} -5, & -8, & -6, & 6, & -1, & 2, & 1, & -5, & 9, & -5 \\ -8, & -5, & -7, & -9, & -3, & -2, & -2, & -10, & 2, & -1 \end{bmatrix} \tag{34b}$$

$$\overline{\mathbf{Y}}_2 = \begin{bmatrix} -0.17, & -0.42, & 0.22, & -0.07, & 0.21, & -0.15, & 0.55, & -0.72, & -0.49, & -0.34 \\ 0.42, & 0.17, & 0.98, & 0.73, & 0.48, & 0.08, & -0.43, & -0.14, & 0.56, & 0.91 \end{bmatrix} \tag{34c}$$

$$\overline{\mathbf{Y}}_3 = \begin{bmatrix} -0.07, & -0.02, & 0.02, & -0.01, & 0.01, & -0.05, & 0.05, & -0.02, & -0.09, & -0.04 \\ 0.02, & 0.07, & 0.08, & 0.03, & 0.08, & 0.1, & -0.03, & -0.04, & 0.06, & 0.01 \end{bmatrix} \tag{34d}$$

V. Performance Bounds and Computational Complexity

In this section, we discuss the theoretical performance bounds of the proposed data model in the form of Cramér-Rao Lower Bounds or CRLB. These bounds are then used during simulations in Section VI as benchmarks to compare the performance of the proposed estimators. We also discuss the computational complexity of the proposed algorithms.

A. Cramér-Rao Lower Bounds

We begin by writing the data model for the transformed measurement $\breve{\mathbf{g}}$, obtained by double centering and half-vectorizing the pairwise distance measurements, and the associated noise covariance, as derived in Appendix A

$$\breve{\mathbf{g}} = \mathbf{g} + \boldsymbol{\eta}_{\mathbf{g}}, \tag{44}$$

where the noise covariance is defined as $\boldsymbol{\Sigma}_{\mathbf{g}} = \mathbb{E}[\boldsymbol{\eta}_{\mathbf{g}}\, \boldsymbol{\eta}_{\mathbf{g}}^T]$. The covariance matrix for $\boldsymbol{\theta}$ in (11) is derived in Appendix A.

Given the noise model in (44), the CRLB for the vectorized form of the relative kinematics parameter $\mathbf{z} \in \{\mathbf{y}_0, \mathbf{y}_1, \ldots\}$, is given by

$$\mathbb{E}\left[\widehat{\mathbf{z}} - \mathbf{z}\right] \geqslant \mathbf{F}_z^{\dagger}, \tag{45}$$

where $\mathbb{E}[\cdot]$ is the expectation operator and $\mathbf{F}_z$ is the associated Fisher information matrix given by

$$\mathbf{F}_z = \mathbf{J}_z^T\, \boldsymbol{\Sigma}_b^{-1}\, \mathbf{J}_z, \tag{46}$$

where $\mathbf{J}_z$ is the Jacobian w.r.t. the parameter to be estimated. For relative position, $\mathbf{Y}_0$, and relative acceleration, $\mathbf{Y}_2$, the covariance matrix $\boldsymbol{\Sigma}_b$ for half-vectorized polynomial coefficients $\{\mathbf{b}_1, \mathbf{b}_3\}$ can be obtained from (56) in Appendix A and the Jacobian $\mathbf{J}_z$ can be calculated using the procedure laid out in Appendix B. For relative velocity, $\mathbf{Y}_1$ and orientation $\mathbf{H}_2$, the Fisher information matrix, $\mathbf{F}_z$, for the system (16) is derived in Appendix C for the unconstrained case. However, the rotation matrix $\mathbf{H}_2$ must satisfy the orthogonality constraint given by $\mathbf{H}_2^T\, \mathbf{H}_2 = \mathbf{I}_D$. As laid out in [44], the constrained CRLB can be calculated as

$$\mathbb{E}\left[\widehat{\mathbf{z}} - \mathbf{z}\right] \geqslant \mathbf{U}\, \left(\mathbf{U}^T\, \mathbf{F}_z\, \mathbf{U}\right)^{-1}\, \mathbf{U}^T, \tag{47}$$

where $\mathbf{U}$ is a matrix whose columns form the orthonormal basis for the null space of the Jacobian of the constraint matrix. For the modified data model in Section IV-D, the induced distribution on the new measurements $\widetilde{\mathbf{r}}$ in (40) results in Chi-squared distribution. This complicates the derivation of CRLB and thus, is not dealt with any further.

B. Computational Complexity

In this section we discuss the asymptotic computational complexity of the proposed algorithms. For Algorithm 1, the computational complexity of the proposed estimator is determined by the least squares solution step 3, (12). Given $\boldsymbol{\theta} \in \mathbb{R}^{\overline{N}(L+1)}$ with $\overline{N} = N(N+1)/2$, for fixed L, the computational complexity of the inversion operation is $\mathcal{O}(N^6)$ and the matrix multiplication is $\mathcal{O}(N^{4\tilde{}}T)$ in the number of mobile nodes. The computational complexity for classical multidimensional scaling algorithm, as implemented in step 4, is governed by the computational complexity of the eigenvalue decomposition of the chosen matrix coefficient $\mathbf{B}_l$ which is given by $\mathcal{O}(N^3)$ in the number of mobile nodes. In the proposed solving scheme in step 5 for a pair of Lyapunov equations, the computational complexity is dictated by the solution to the constrained least-squares solution in (25) and is given by $\mathcal{O}(N^3 D^6)$. Thus, for large networks, the asymptotic complexity is dominated by the number of nodes in the network N. For small networks, the length of the times series determines the computational complexity. For Algorithm 2, we need an additional computation for the estimation of matrix coefficients $\widehat{\mathbf{Y}}_l$, $l \geq 2$ from centered accelerometer data in step 3, which has the computational complexity of $\mathcal{O}(N^3 D^3)$ for a fixed order L of the polynomial trajectory owing to the inversion of matrix $\mathbf{V}$ in (36).

VI. Simulation

For the simulation setup, we consider a scenario with $N = 10$ mobile nodes in $D = 2$ dimensions, with the absolute kinematics matrix coefficients, $\mathbf{Y}_l$, given in (34). The noise in the measurements, pairwise distance and accelerometer, are modeled as zero-mean Gaussian noise with a standard deviation of $\sigma_d = 0.01\ m$ [26], [45] and $\sigma_a = 0.001\ m/s^2$ respectively. A total of $N_{\text{exp}} = 1000$ Monte-Carlo runs were executed. Let $\widehat{\mathbf{Z}}(n)$ represent the relative kinematic parameter estimate for the nth Monte-Carlo run, where $\mathbf{Z} \in \{\mathbf{Y}_0, \mathbf{Y}_1, \mathbf{Y}_2\}$. The Root-Mean-Square-Error (RMSE) for the parameters of interest, $\mathbf{Z}$, is computed as

$$\text{RMSE}(\mathbf{Z}) = N_z^{-1} \left(\sqrt{N_{\text{exp}}^{-1} \sum_{n=1}^{N_{\text{exp}}} \left\| \text{vech}\left(\mathbf{H}\, \widehat{\mathbf{Z}}(n) - \mathbf{Z}\right) \right\|^2} \right), \tag{48}$$

where $\mathbf{H}$ is the optimal Procrustes rotation calculated for the nth Monte-Carlo run. For the CRLB, the root-mean-square-error is calculated as

$$\text{RMSE}(\mathbf{Z}) = \frac{1}{ND}\, \left(\text{Tr}\left(\mathbf{F}_{\mathbf{Z}}^{-1}\right)\right)^{1/2}, \tag{49}$$

where $\text{Tr}(\cdot)$ is the trace operator and $\mathbf{F}_{\mathbf{Z}}$ is the appropriate Fisher information matrix corresponding to parameter $\mathbf{Z}$. All simulations are performed for a fixed time interval of $\Delta T = [-5, 5]$ seconds with a varying range of K. The code for the simulation carried out in this work can be found on Github [46].

In Section VI-A, the relative kinematic estimates using the proposed data model are compared against the state of the art [36] for the constant velocity case. The Cramér-Rao bounds of the proposed algorithm is compared with the bound derived for [36] for these estimates. Section VI-B provides the simulation results for the constant acceleration case together with the Cramér-Rao bounds. Section VI-C discusses the effect of signal-to-noise ratio (SNR) for distance and accelerometer measurements. Unless otherwise stated, SNR is calculated as $-10\ \log_{10}(\sigma)$, where σ is the standard deviation for the parameter under consideration.

A. Constant Velocity Scenario

Fig. 1(a) compares the RMSE for the estimates of the relative kinematics solution for the constant velocity case, w.r.t. the State-of-the-Art (SOTA) in [36, Sections 3.4 and 4.1]. The proposed data model shows a lower root mean square error

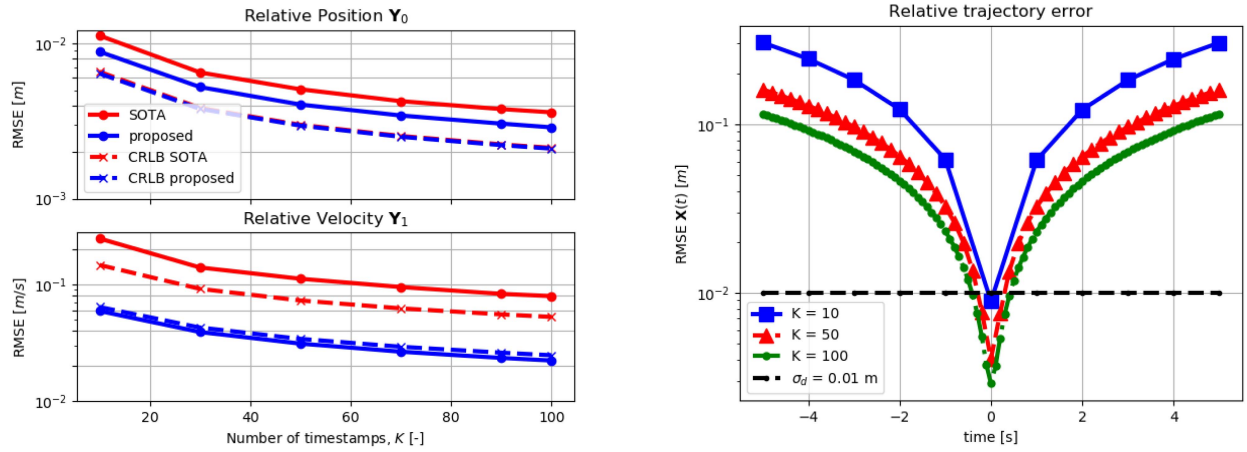

(a) (b)

Fig. 1. a) RMSE for relative position and relative velocity for the constant velocity case as compared to the State of the Art (SOTA) [34], at $t = 0$ for varying K. b) RMSE for position estimates over time.

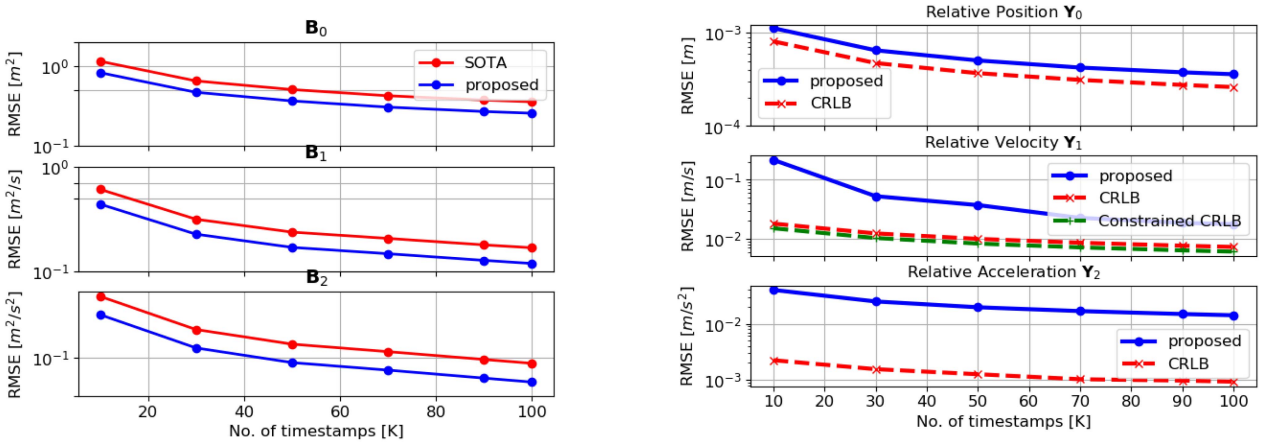

(a) (b)

Fig. 2. RMSE for a) Grammian polynomial coefficient from (9) b) relative position, relative velocity and relative acceleration at $t = 0$ and the corresponding CRLB (47), for varying K. The corresponding State Of The Art (SOTA) [36] results are plotted for comparison.

(RMSE) for all coefficient estimates compared to [36]. The CRLBs for the proposed estimator (45) and SOTA [36, Section 6.2] are also shown. For $\mathbf{Y}_0$, the CRLB for the proposed data model almost overlaps with the SOTA as the underlying noise model is the same. The slight difference can be attributed to the approximation of the noise model as laid out in Appendix A. The CRLB for $\mathbf{Y}_1$ shows a significant improvement over the SOTA. The proposed estimator seems to achieve the CRLB for the constant velocity case. However, the slight difference between the two blue curves can be attributed to the approximation in the noise model. It should also be noted that Fig. 1(b) shows the RMSE of position estimates using the proposed model over time for various values of K. The accuracy of the estimates decreases as one moves away from $t = 0$ as the Taylor approximation gets worse away from the point of approximation.

B. Constant Acceleration Scenario

As previously discussed, the estimation of relative kinematics in the SOTA in [36] requires additional rigid body constraints. Thus, it is more insightful to compare the polynomial coefficients, $\mathbf{B}_l$ in (8) of the proposed method with the methodology given in [36]. Fig. 2(a) shows the comparison in terms of RMSE of the coefficients $\mathbf{B}_l$ between the proposed method and the SOTA. Fig. 2(b) shows the RMSE for the estimates of the relative position, velocity and acceleration at time $t = 0$ for varying K. The CRLBs for the relative kinematics are also plotted for the relative kinematic parameters, as given in Section V-A. The performance gap between the proposed estimator and the theoretical bound decreases as the number of samples increases. A joint estimation approach may potentially lead to close-to-optimal performance. Finally, Fig. 5 shows the effect of adding accelerometer measurements by modifying the data model under the assumption laid out in (33). The addition of the accelerometer significantly improves the estimation of relative kinematic parameters.

C. Effect of Signal-to-Noise Ratio

In this subsection, we consider the role of noise on the proposed estimators. Fig. 3 shows the RMSE errors as a function

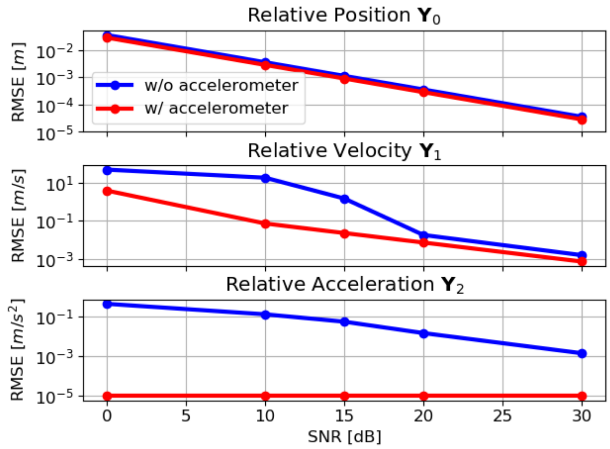

Fig. 3. RMSE for relative kinematics for varying SNR on the pairwise distances at $t = 0$.

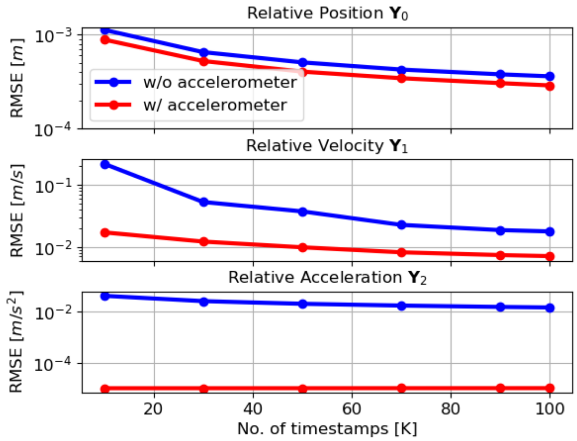

Fig. 5. a) RMSE for the relative position, relative velocity and relative acceleration at $t = 0$ with (w/) and without (w/o) accelerometer measurements, for varying K.

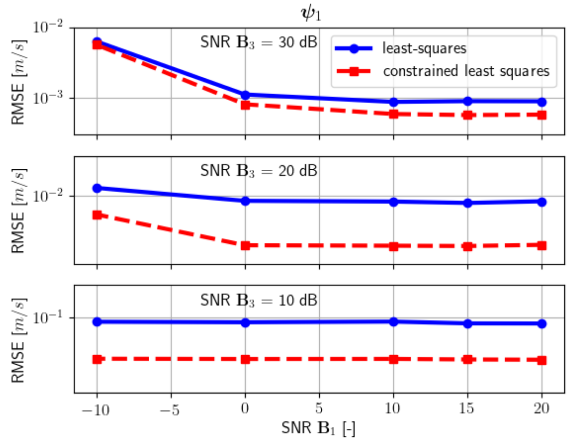

Fig. 4. RMSE for the approximation error in (51) for different SNR values.

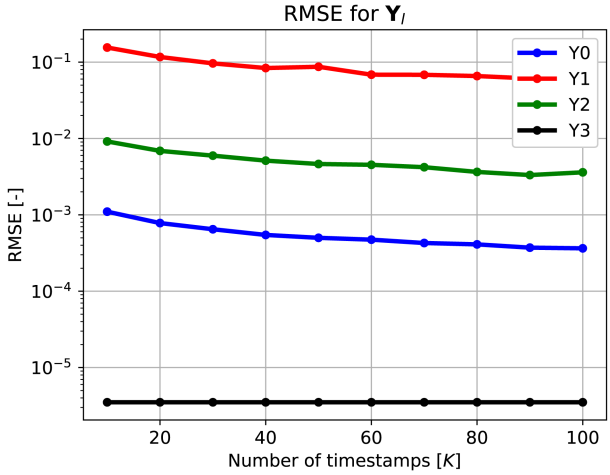

Fig. 6. RMSE of relative kinematic parameters for a general trajectory with $L = 3$ for varying K in the presence of accelerometer measurements.

of signal-to-noise ratio (SNR) on the pairwise distances. Here, the standard deviation, σ_d for the pairwise distances is varied between 1m and 0.01m with the corresponding SNR value given by $-10\ \log(\sigma_d)$ dB. The RMSE value for the estimates decreases as the SNR increases, as expected.

In particular, the error corresponding to the relative velocity, $\mathbf{Y}_1$ is significantly affected by the noise on the pairwise distances as shown by the blue curve. The nonlinear trendline for the case without accelerometer is due to the fact that there is noise on both the coefficient estimates $\widehat{\mathbf{B}}_l,\ l \in \{1, 3\}$ and the kinematic estimates $\widehat{\mathbf{Y}}_m,\ m \in \{0, 2\}$ in (16). However, this effect is less pronounced when accelerometer measurements are included, as shown by the red curve. The errors in the estimates of $\mathbf{Y}_0$ and $\mathbf{Y}_2$ negatively affect the accuracy of $\mathbf{Y}_1$ estimate. This is apparent in the form of (15) which relies on these estimates. With an improvement in the estimate of $\mathbf{Y}_2$ using accelerometer measurements, the RMSE for $\mathbf{Y}_1$ improves significantly.

As discussed in Section IV-C, for constant but distinct orientation of the accelerometer sensor on the mobile nodes, one can estimate the relative orientations of the individual sensors by solving the constrained least squares formulation in (37). However, the extremely low signal-to-noise ratio for the estimated polynomial coefficient $\widehat{\mathbf{B}}_4$ makes it impractical.

For the estimators proposed in (24) and (25), we apply Gaussian noise directly on $\mathbf{B}_1$ and $\mathbf{B}_3$ in (16). Fig. 4 shows the comparison between the two approaches for the estimate of $\boldsymbol{\psi}_1$ in (23). The noise on $\mathbf{B}_3$ significantly affects the RMSE compared to the noise on $\mathbf{B}_1$ since the entries of $\mathbf{B}_3$ have smaller values leading to worse SNR. The constrained least squares leads to better estimates as the data gets noisier.

D. General Polynomial Trajectory Scenario

For the general trajectory case, it is assumed that the mobile nodes follow a polynomial trajectory of order $L = 3$. We begin with the case where accelerometer measurements are available. Fig. 6 shows the RMSE of the relative kinematic parameter estimates for varying values of K, as laid out in Section IV

and Algorithm 2. Similar to the constant velocity and acceleration scenarios, the RMSE decreases with increasing number of samples K. In general, the proposed algorithm can estimate the relative kinematic parameters in polynomial trajectories of any given order L, in the presence of accelerometer measurements.

In the case where only pairwise distance measurements are available, the general polynomial trajectory scenario can be extended using an adaptive filter, which is the subject of ongoing research. There are a number of challenges associated with the design of such a filter. One such challenge is in the estimation of higher-order matrix coefficients $\mathbf{B}_l$, $l > 2$ in (8), which are severely affected by the noise levels in the pairwise distance measurements. This in turn affects the estimates of relative velocity $\mathbf{Y}_1$ and relative acceleration $\mathbf{Y}_2$. Another challenge is related to the fact that the position estimates, for each time window, give only the shape of the network in space for the given window, i.e. the relative position of the nodes w.r.t. the centroid of the network. In order to establish a relationship between $\mathbf{Y}_0$ over different time windows, a prediction and update step is required together with the associated convergence analysis. A complete analysis of the details of the adaptive filter is outside the scope of the presented work.

VII. Conclusions & Future Works

In this paper, a Grammian-based formulation to the problem of estimating the relative kinematics given time-varying pairwise distances between mobile nodes is presented. The proposed method meets the state-of-the-art on the estimation of relative position and improves on the accuracy for relative velocity estimation in anchorless scenarios. Furthermore, the proposed method estimates the relative acceleration and higher-order parameters without the requirement of any rigid body constraints. Cramér-Rao bounds for the proposed data model are compared against the state-of-the-art and simulations are provided to show the performance of the proposed approach against the state-of-the-art to highlight the effectiveness of the proposed data model. The inclusion of accelerometer measurements, under the assumption of a non-rotating accelerometer frame, considerably improves the relative kinematic estimates.

For future work, we aim to implement the proposed estimators on practical datasets with mobile nodes such as [47], [48]. Another direction for future investigation is the design of an adaptive filter using the second-order polynomial approximation presented in Section III and the associated convergence analysis based on the challenges mentioned in Section VI-D. Moreover, we have considered constant non-rotating frames of reference for the accelerometer measurements, which limits the applicability of the proposed approach to only holonomic systems. For a more general approach, additional information about the orientation of the accelerometers is required to model the relationship between these measurements over time. Our work can serve as a base case study in this direction. Another research direction is to formulate a joint approach, combining pairwise distances and accelerometer measurements, into a common data model. This can lead to a more efficient estimator and improve upon the work presented here. Additionally, the denoising approach in [37] to get less noisy Grammian matrices and 'Divide-and-Conquer' approach proposed in [49] can further improve these results with comparatively little effort.

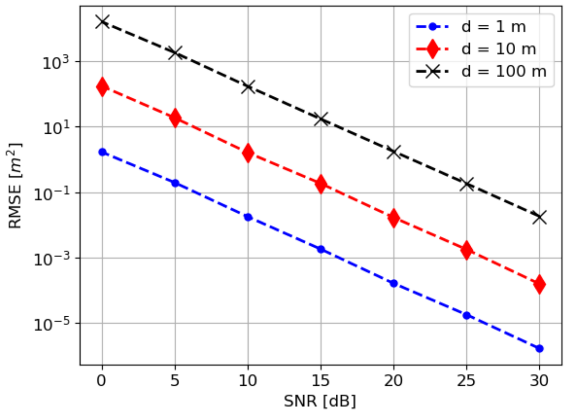

Fig. 7. RMSE for the approximation error in (51) for different SNR values, where SNR is defined to be $10\log_{10}(\frac{d}{\eta})$.

Appendix A
Noise Models

In this section, we assume a Gaussian white noise model for the pairwise distances in EDM, $\mathbf{D}_k$, and derive the noise models for the proposed data models with and without accelerometer measurements.

A. Noise Model for $\check{\mathbf{g}}$ in (11)

We assume an additive white Gaussian noise model for the pairwise distance measurements $d_{ij,k}$ [36], given by

$$\check{d}_{ij,k} = d_{ij,k} + \eta_{ij,k}, \tag{50}$$

where $\check{d}_{ij,k}$ is the noisy measurement and $\eta_{ij,k} \sim \mathcal{N}(0, \sigma_d^2)$. Squaring (50), we get

$$\check{d}^2_{ij,k} = d^2_{ij,k} + \eta^2_{ij,k} + 2\, d_{ij,k}\, \eta_{ij,k} \tag{51a}$$

$$\approx d^2_{ij,k} + 2\, d_{ij,k}\, \eta_{ij,k}. \tag{51b}$$

The error in approximation of the squared distance is shown in Fig. 7 for various distance values and SNR values. The validity of the approximation would depend on the application chosen. Stacking the squared distances, we get

$$\check{\mathbf{d}}_k^{\odot 2} = \mathbf{S}\ \mathrm{vec}(\check{\mathbf{D}}_k) = \mathbf{d}_k^{\odot 2} + 2\ \mathrm{diag}(\mathbf{d}_k)\, \boldsymbol{\eta}_k, \tag{52}$$

where $\check{\mathbf{D}}_k$ is the noisy EDM at time t_k with $\mathbf{S}$ as the full row-rank selection matrix for selecting the unique non-zero elements of $\check{\mathbf{D}}_k$. Here, $\mathbf{d}_k \triangleq [d_{ij,k}], \forall i, j \leq N; i \leq j$ is the stacked pairwise distances at time t_k. The covariance matrix for the data model in (52) is given by $\boldsymbol{\Sigma}_{\mathbf{d}_k} = 4\ \mathrm{diag}(\mathbf{d}_k)\, \Sigma_d\ \mathrm{diag}(\mathbf{d}_k) \in \mathbb{R}^{\overline{N}\times\overline{N}}$ with $\Sigma_d = \mathbb{E}[\boldsymbol{\eta}_k\, \boldsymbol{\eta}_k^T] = \sigma_d^2\, \mathbf{I}_{\overline{N}}$.

Now, rewriting the expression for the Grammian, $\mathbf{G}_k$, from (7), we get

$$\mathrm{vec}(\mathbf{G}_k) = -\frac{1}{2}\ \left(\mathbf{C}^T \otimes \mathbf{C}\right)\ \mathrm{vec}(\mathbf{D}_k). \tag{53}$$

Substituting (52) in (53), the half-vectorized Grammian, $\mathbf{g}_k$, can be written as

$$\mathbf{g}_k = \mathbf{M}\, \mathbf{d}_k^{\odot 2}, \tag{54}$$

where $\mathbf{M} = -\frac{1}{2}\, \mathbf{L}\, (\mathbf{C}^T \otimes \mathbf{C})\, \mathbf{S}^{\dagger}$, $\mathbf{L} \in \mathbb{R}^{\overline{N} \times N^2}$ is the elimination matrix and $\mathbf{S}^{\dagger}$ is the Moore-Penrose pseudo-inverse of $\mathbf{S}$. Using (54) and the data model for $\text{vech}(\mathbf{D}_k)$ from (52), the data model for noisy $\mathbf{g}_k$ can be written as $\check{\mathbf{g}}_k = \mathbf{g}_k + \boldsymbol{\eta}_{\mathbf{g}_k}$ with the noise covariance matrix, $\boldsymbol{\Sigma}_{\mathbf{g}_k} = \mathbb{E}[\boldsymbol{\eta}_{\mathbf{g}_k}^T\, \boldsymbol{\eta}_{\mathbf{g}_k}] = \mathbf{M}\, \boldsymbol{\Sigma}_{\mathbf{D}_k}\, \mathbf{M}^T$. Stacking together the K timestamps, the noise model for transformed measurements $\check{\mathbf{g}}$ from (11) is given by

$$\check{\mathbf{g}} = \mathbf{g} + \boldsymbol{\eta}_{\mathbf{g}}, \tag{55}$$

with $\boldsymbol{\Sigma}_{\mathbf{g}} = \mathbb{E}[\boldsymbol{\eta}_{\mathbf{g}}^T\, \boldsymbol{\eta}_{\mathbf{g}}] = \text{diag}(\boldsymbol{\Sigma}_{\mathbf{g}_0}, \boldsymbol{\Sigma}_{\mathbf{g}_1}, \ldots, \boldsymbol{\Sigma}_{\mathbf{g}_K})$. The diagonal structure for the covariance matrix is justified under the assumption that the measurements at different timestamps are independent. Given $\boldsymbol{\Sigma}_{\mathbf{g}}$, the covariance matrix for the coefficient estimates $\boldsymbol{\theta}$ in (11) is given by $\boldsymbol{\Sigma}_{\boldsymbol{\theta}} = \mathbf{T}^T\, \boldsymbol{\Sigma}_{\mathbf{g}}\, \mathbf{T}$. For later use, we split this covariance matrix as

$$\boldsymbol{\Sigma}_{\boldsymbol{\theta}} = \begin{bmatrix} \boldsymbol{\Sigma}_{00}, & \boldsymbol{\Sigma}_{01}, & \ldots, & \boldsymbol{\Sigma}_{0L} \\ \boldsymbol{\Sigma}_{10}, & \boldsymbol{\Sigma}_{11}, & \ldots, & \boldsymbol{\Sigma}_{1L} \\ \vdots, & & \ddots, & \vdots \\ \boldsymbol{\Sigma}_{L0}, & \boldsymbol{\Sigma}_{L1}, & \ldots, & \boldsymbol{\Sigma}_{LL} \end{bmatrix}, \tag{56}$$

where $\boldsymbol{\Sigma}_{ij}$ denotes the covariance between half-vectorized polynomial coefficients $\mathbf{b}_i$ and $\mathbf{b}_j$ in (10).

B. Noise Model for $\widetilde{\mathbf{r}}$ in (41)

For the data model in (40), we rewrite the expression for the *modified* measurement in (39),

$$\widetilde{\mathbf{r}} = \text{vec}(\widetilde{\mathbf{G}}) = \check{\mathbf{g}} - \text{vec}\left(\sum_{l=2}^{L} (l!)^{-2}\, \widetilde{\mathbf{Y}}_l^T\, \widetilde{\mathbf{Y}}_l \right). \tag{57}$$

Similar to the noise model for $\check{\mathbf{g}}$ in (55), one can approximate the noise for the second term in (57) using a heteroskedastic Gaussian distribution. Consequently, the noise model for $\widetilde{\mathbf{r}}$ can be written as a sum of two heteroskedastic Gaussian variables.

Appendix B
Cramér-Rao Lower Bounds for Relative Position and Relative Acceleration for (14)

Following the derivations in [35], consider the following general formulation for estimating unknown kinematic parameter $\mathbf{y} \triangleq \text{vec}(\mathbf{Y}) = \begin{bmatrix} \mathbf{y}_1^T, & \ldots, & \mathbf{y}_N^T \end{bmatrix}^T \in \mathbb{R}^{ND \times 1}$ in (14) from estimates, denoted as $\mathbf{b} \in \mathbb{R}^{\overline{N}}$,

$$\mathbf{b} = \mathbf{s}(\mathbf{y}) + \boldsymbol{\eta}_b, \tag{58}$$

where $\mathbf{b} \in \mathbb{R}^{\overline{N}}$ with $\overline{N} = \frac{N(N+1)}{2}$. The form of the nonlinear equation $\mathbf{s}(\mathbf{y})$ in (14) is given as $\mathbf{s}(\mathbf{y}) = \begin{bmatrix} s(\mathbf{y}_1, \mathbf{y}_1), & s(\mathbf{y}_1, \mathbf{y}_2), & \ldots, & s(\mathbf{y}_N, \mathbf{y}_N) \end{bmatrix}^T$ with $s(\mathbf{y}_i, \mathbf{y}_j) = \mathbf{y}_i^T\, \mathbf{y}_j$. To get the noise on $\boldsymbol{\Sigma}_b = \mathbb{E}[\boldsymbol{\eta}_b^T\, \boldsymbol{\eta}_b]$ on the coefficient estimates in (14), consider the covariance matrix in (56). Based on the parameter under consideration in (14), the corresponding conditional covariance matrix can be easily evaluated. The Fisher information matrix is given by

$$\mathbf{F}_{\mathbf{y}} = \left(\frac{\partial \mathbf{s}(\mathbf{y})}{\partial \mathbf{y}} \right)^T\, \boldsymbol{\Sigma}_b^{-1}\, \left(\frac{\partial \mathbf{s}(\mathbf{y})}{\partial \mathbf{y}} \right), \tag{59}$$

where the Jacobian matrix for $\mathbf{s}(\mathbf{y})$ with respect to $\mathbf{y}$, is given by $\frac{\partial \mathbf{s}(\mathbf{y})}{\partial \mathbf{y}} = \begin{bmatrix} \frac{\partial \mathbf{s}(\mathbf{y})}{\partial \mathbf{y}_1}, & \ldots, & \frac{\partial \mathbf{s}(\mathbf{y})}{\partial \mathbf{y}_N} \end{bmatrix}$, where $\frac{\partial \mathbf{s}(\mathbf{y})}{\partial \mathbf{y}_i} = \begin{bmatrix} \frac{\partial s(\mathbf{y}_1, \mathbf{y}_1)}{\partial \mathbf{y}_i}, & \frac{\partial s(\mathbf{y}_1, \mathbf{y}_2)}{\partial \mathbf{y}_i}, & \ldots, & \frac{\partial s(\mathbf{y}_N, \mathbf{y}_N)}{\partial \mathbf{y}_i} \end{bmatrix}$, with

$$\frac{\partial s(\mathbf{y}_j, \mathbf{y}_k)}{\partial \mathbf{y}_i} = \begin{cases} \mathbf{y}_k^T & \text{if } i = j \\ \mathbf{y}_j^T & \text{if } i = k \\ 2\, \mathbf{y}_i^T & \text{otherwise.} \end{cases} \tag{60}$$

The inverse of the Fisher information matrix gives the desired lower bound.

Appendix C
Cramér-Rao Lower Bound - Relative Velocity and Rotation for (16) and (43)

Consider matrices $\mathbf{A}, \mathbf{C}, \mathbf{X} \in \mathbb{R}^{M \times N}$ such that $M < N$. Additionally, matrices $\mathbf{P}, \mathbf{Q} \in \mathbb{R}^{N \times N}$ are positive-definite symmetric matrices. Consider the pair of Lyapunov-like equations, similar to the one given in (16),

$$\mathbf{A}^T\, \mathbf{X} + \mathbf{X}^T\, \mathbf{A} = \mathbf{P}, \tag{61a}$$

$$\mathbf{C}^T\, \mathbf{H}\, \mathbf{X} + \mathbf{X}^T\, \mathbf{H}^T\, \mathbf{C} = \mathbf{Q}, \tag{61b}$$

where $\mathbf{H}^T\, \mathbf{H} = \mathbf{I}$. We define $\mathbf{h} \triangleq \text{vec}(\mathbf{H})$. Let $\mathbf{z} = \begin{bmatrix} \mathbf{x}^T & \mathbf{h}^T \end{bmatrix}^T$ where $\mathbf{x} = \text{vec}(\mathbf{X}) = \begin{bmatrix} \mathbf{x}_1^T & \ldots & \mathbf{x}_N^T \end{bmatrix}^T$. The system model can be written as

$$\mathbf{r} = \begin{bmatrix} \text{vech}(\mathbf{P}) \\ \text{vech}(\mathbf{Q}) \end{bmatrix} = \begin{bmatrix} \mathbf{s}_p(\mathbf{z}) \\ \mathbf{s}_q(\mathbf{z}) \end{bmatrix} + \begin{bmatrix} \boldsymbol{\eta}_p \\ \boldsymbol{\eta}_q \end{bmatrix}, \tag{62}$$

where

$$\mathbf{s}_p(\mathbf{z}) = \begin{bmatrix} s_p(\mathbf{x}_1, \mathbf{x}_1), s_p(\mathbf{x}_1, \mathbf{x}_2), \ldots, s_p(\mathbf{x}_N, \mathbf{x}_N) \end{bmatrix}^T,$$

$$\mathbf{s}_q(\mathbf{z}) = \begin{bmatrix} s_q(\mathbf{x}_1, \mathbf{x}_1, \mathbf{h}), s_q(\mathbf{x}_1, \mathbf{x}_2, \mathbf{h}), \ldots, s_q(\mathbf{x}_N, \mathbf{x}_N, \mathbf{h}) \end{bmatrix}^T,$$

and $s_p(\mathbf{x}_i, \mathbf{x}_j) = \mathbf{a}_i^T\, \mathbf{x}_j + \mathbf{x}_i^T\, \mathbf{a}_j$, $s_q(\mathbf{x}_i, \mathbf{x}_j, \mathbf{h}) = \mathbf{c}_i^T\, \mathbf{H}\, \mathbf{x}_j + \mathbf{x}_i^T\, \mathbf{H}^T\, \mathbf{c}_j$. Here, $\boldsymbol{\Sigma}_r = \mathbb{E}[\boldsymbol{\eta}_r^T\, \boldsymbol{\eta}_r]$ can be evaluated from (56). The corresponding Fisher information matrix for the joint estimation of $\mathbf{x}$ and $\mathbf{h}$ is given by

$$\mathbf{F}_{\mathbf{z}} = \left(\frac{\partial \mathbf{s}(\mathbf{z})}{\partial \mathbf{z}} \right)^T\, \boldsymbol{\Sigma}_r^{-1}\, \left(\frac{\partial \mathbf{s}(\mathbf{z})}{\partial \mathbf{z}} \right). \tag{63}$$

The Jacobian matrix for $\mathbf{s}(\mathbf{z})$ with respect to $\mathbf{z}$, is given by $\frac{\partial \mathbf{s}(\mathbf{z})}{\partial \mathbf{z}} = \begin{bmatrix} \frac{\partial \mathbf{s}_p(\mathbf{z})}{\partial \mathbf{z}}, & \frac{\partial \mathbf{s}_q(\mathbf{z})}{\partial \mathbf{z}} \end{bmatrix}$, where

$$\frac{\partial \mathbf{s}_p(\mathbf{z})}{\partial \mathbf{z}} = \begin{bmatrix} \frac{\partial \mathbf{s}_p(\mathbf{z})}{\partial \mathbf{x}_1}, & \ldots, & \frac{\partial \mathbf{s}_p(\mathbf{z})}{\partial \mathbf{x}_N}, & \mathbf{0} \end{bmatrix},$$

$$\frac{\partial \mathbf{s}_q(\mathbf{z})}{\partial \mathbf{z}} = \begin{bmatrix} \frac{\partial \mathbf{s}_q(\mathbf{z})}{\partial \mathbf{x}_1}, & \ldots, & \frac{\partial \mathbf{s}_q(\mathbf{z})}{\partial \mathbf{x}_N}, & \frac{\partial \mathbf{s}_q(\mathbf{z})}{\partial \mathbf{h}} \end{bmatrix}.$$

The derivatives $\frac{\partial \mathbf{s}_p(\mathbf{z})}{\partial \mathbf{x}_i}$, $\frac{\partial \mathbf{s}_q(\mathbf{z})}{\partial \mathbf{x}_i}$ and $\frac{\partial \mathbf{s}_q(\mathbf{z})}{\partial \mathbf{h}}$ are given by

$$\frac{\partial \mathbf{s}_p(\mathbf{z})}{\partial \mathbf{x}_i} = \left[\frac{\partial s_p(\mathbf{x}_1,\mathbf{x}_2)}{\partial \mathbf{x}_i}, \quad \ldots, \quad \frac{\partial s_p(\mathbf{x}_{N-1},\mathbf{x}_N)}{\partial \mathbf{x}_i}\right],$$

$$\frac{\partial \mathbf{s}_q(\mathbf{z})}{\partial \mathbf{x}_i} = \left[\frac{\partial s_q(\mathbf{x}_1,\mathbf{x}_2,\mathbf{h})}{\partial \mathbf{x}_i}, \quad \ldots, \quad \frac{\partial s_q(\mathbf{x}_{N-1},\mathbf{x}_N,\mathbf{h})}{\partial \mathbf{x}_i}\right],$$

with

$$\frac{\partial s_p(\mathbf{x}_i,\mathbf{x}_j)}{\partial \mathbf{x}_k} = \begin{cases} 2\,\mathbf{a}_i^T & \text{if } k=i=j \\ \mathbf{a}_j^T & \text{if } k=i\neq j \\ \mathbf{a}_i^T & \text{if } k=j\neq i \\ \mathbf{0}^T & \text{otherwise,} \end{cases}$$

$$\frac{\partial s_q(\mathbf{x}_i,\mathbf{x}_j,\mathbf{h})}{\partial \mathbf{x}_k} = \begin{cases} 2\,\mathbf{c}_i^T\,\mathbf{H} & \text{if } k=i=j \\ \mathbf{c}_j^T\,\mathbf{H} & \text{if } k=i \\ \mathbf{c}_i^T\,\mathbf{H} & \text{if } k=j \\ \mathbf{0}^T & \text{otherwise,} \end{cases}$$

$$\frac{\partial s_q(\mathbf{x}_1,\mathbf{x}_2,\mathbf{h})}{\partial \mathbf{h}_k} = \begin{cases} \mathbf{c}_i^T\,\mathbf{x}_j + \mathbf{x}_i^T\,\mathbf{c}_j & \text{if } k=i \\ \widetilde{\mathbf{c}}_i^T\,\mathbf{x}_j + \mathbf{x}_i^T\,\widetilde{\mathbf{c}}_j & \text{if } k=j \\ \mathbf{0}^T & \text{otherwise,} \end{cases}$$

where $\widetilde{\mathbf{c}}_i$ is appropriately defined based on M.

Appendix D
Solvability of Lyapunov-Like Equations

As discussed in Section III-B, for a pair of equations of the form in (15) and its subsequent reduced form in (23), the aspects related to the solvability of such a pair of equations is discussed here. We begin by rewriting (22),

$$\begin{bmatrix} \overline{\boldsymbol{\psi}}_1 \\ \overline{\boldsymbol{\psi}}_2 \\ \overline{\boldsymbol{\phi}} \end{bmatrix} = \overline{\mathbf{K}}\ (\mathbf{I}\otimes\mathbf{H}_2)\ \mathbf{K} \begin{bmatrix} \boldsymbol{\psi}_1 \\ \boldsymbol{\psi}_2 \\ \boldsymbol{\phi} \end{bmatrix}, \tag{64}$$

where $\overline{\mathbf{K}} \triangleq \overline{\mathbf{V}}^T \otimes \overline{\mathbf{U}}^T$ and $\mathbf{K} \triangleq \mathbf{V}\otimes\mathbf{U}$. The above equation can be rearranged to yield

$$\begin{bmatrix} \overline{\boldsymbol{\psi}}_2 \\ \overline{\boldsymbol{\phi}} \end{bmatrix} = \mathbf{W}\,\boldsymbol{\xi}(\boldsymbol{\psi}_1,\mathbf{h}_2), \tag{65}$$

To see this, we split matrices $\overline{\mathbf{K}}$ and $\mathbf{K}$ in blocked form as follows

$$\overline{\mathbf{K}} = \begin{bmatrix} \overline{\mathbf{K}}_{11}, & \ldots, & \overline{\mathbf{K}}_{1N} \\ \vdots, & \ddots, & \vdots \\ \overline{\mathbf{K}}_{N1}, & \ldots, & \overline{\mathbf{K}}_{NN} \end{bmatrix}, \mathbf{K} = \begin{bmatrix} \mathbf{K}_{11}, & \ldots, & \mathbf{K}_{1N} \\ \vdots, & \ddots, & \vdots \\ \mathbf{K}_{N1}, & \ldots, & \mathbf{K}_{NN} \end{bmatrix},$$

where $\mathbf{K}_{ij} \in \mathbb{R}^{D\times D}$. Expanding further, we get

$$\begin{bmatrix} \overline{\boldsymbol{\psi}}_1 \\ \overline{\boldsymbol{\psi}}_2 \\ \overline{\boldsymbol{\phi}} \end{bmatrix} = \begin{bmatrix} \mathbf{R}_{11}, & \ldots, & \mathbf{R}_{1N} \\ \vdots, & \ddots, & \vdots \\ \mathbf{R}_{N1}, & \ldots, & \mathbf{R}_{NN} \end{bmatrix} \begin{bmatrix} \boldsymbol{\psi}_1 \\ \boldsymbol{\psi}_2 \\ \boldsymbol{\phi} \end{bmatrix}, \tag{66}$$

where $\mathbf{R}_{ij} \triangleq \sum_k \overline{\mathbf{K}}_{ik}\,\mathbf{H}_2\,\mathbf{K}_{kj}$. To recover coefficients corresponding to only known elements of LHS, we consider a row of the equation in (66) where $\psi_1 \in \boldsymbol{\psi}_1$, h_1 and h_2 are unknown but $\psi_2 \in \boldsymbol{\psi}_2$ is known, i.e.

$$\overline{\psi}_1 = \bar{k}_{11}\,h_1\,k_{11}\,\psi_1 + \bar{k}_{12}\,h_2\,k_{11}\,\psi_1 + \bar{k}_{12}\,h_1\,k_{21}\,y_2 - \bar{k}_{12}\,h_2\,k_{21}\,\psi_2,$$

Thus, we can collect the coefficients for the unknown ψ_1, h_1 and h_2, which form the first row of matrix $\mathbf{W}$ in (65).

The invertibility of matrix $\mathbf{W}$ depends upon the ranks of estimates of the Grammian polynomial coefficients, $\mathbf{B}_1, \mathbf{B}_3 \in \mathbb{R}^{\overline{N}\times\overline{N}}$. Since these coefficients correspond to centered polynomial trajectory, the centering operation causes the estimates to lose rank, i.e. the estimated matrices have rank $\overline{N}-1$. However, this rank loss can be compensated for by choosing more nodes. For the given case, the matrix $\mathbf{W}$ is invertible. Among the unknowns, we have $\boldsymbol{\psi}_1 \in \mathbb{R}^{D_1}$ and $\mathbf{h} \in \mathbb{R}^{D_2}$, where $D_1 \triangleq D^2 - D$ and D_2 depends upon the how we formulate the rotation vector $\mathbf{h}$. For D-dimensional space, $D_2 = \binom{D}{2}$ corresponding to the rotational degrees of freedom and $D_2 = D^2$ if no constraints are imposed.

For instance, consider the case for $D=2$. This leads to $\boldsymbol{\psi}_1 \in \mathbb{R}^2$. We further denote the unknowns in rotation matrix $\mathbf{H}_2$ as $\mathbf{h} = \begin{bmatrix} h_1, & h_2 \end{bmatrix}^T$ where $\mathbf{H}_2 = \begin{bmatrix} h_1, & -h_2 \\ h_2, & h_1 \end{bmatrix}$. The number of cross terms in $\boldsymbol{\xi}(\boldsymbol{\psi}_1,\mathbf{h})$ is given by $\binom{D_1+1}{1}\binom{D_2}{1}$. For $D=2$ and $\mathbf{h} = \begin{bmatrix} h_1, & h_2 \end{bmatrix}^T$, the number of cross terms can be calculated as $\binom{3}{1}\binom{2}{1} = 6$, which is given by

$$\boldsymbol{\xi}(\boldsymbol{\psi}_1,\mathbf{h}) = \begin{bmatrix} \xi_1, & \xi_2, & \xi_3, & \xi_4, & \xi_5, & \xi_6 \end{bmatrix}^T \tag{67a}$$

$$= \begin{bmatrix} h_1, & h_2, & h_1,\psi_{1,1}, & h_1,\psi_{1,2}, & h_2,\psi_{1,1}, & h_2,\psi_{1,2} \end{bmatrix}^T, \tag{67b}$$

where $\boldsymbol{\psi}_1 = \begin{bmatrix} \psi_{1,1} & \psi_{1,2} \end{bmatrix}^T$. For $N \geq 4$, (65) is solvable. For the given set of basis function in (67), the unique arguments $\widehat{\boldsymbol{\psi}}_1$ and $\widehat{\mathbf{h}}$ can be calculated as

$$\widehat{h}_1 = \xi_1^*, \quad \widehat{h}_2 = \xi_2^*, \quad \widehat{\psi}_{1,1} = \frac{h_1\,\xi_3^*}{\widehat{h}_1}, \quad \widehat{\psi}_{1,2} = \frac{h_2\,\xi_4^*}{\widehat{h}_2}$$

Hence, uniqueness in $\boldsymbol{\xi}(\boldsymbol{\psi}_1,\mathbf{h})$ implies uniqueness in its arguments, $\boldsymbol{\psi}_1$ and $\mathbf{h}$.

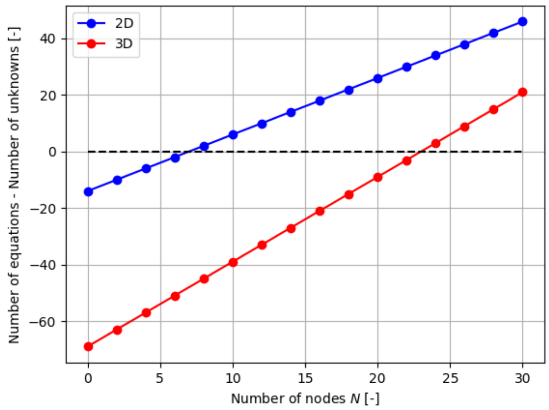

Fig. 8. Conditions for solvability of (65) derived from (15) in Section III-B for both 2D and 3D cases.

Fig. 8 shows the number of nodes required for both 2D and 3D cases. As discussed, solvability depends on the number of mobile nodes available. The number of nodes required can be reduced further by incorporating the constraints, similar to the 2D case, on the rotation vector $\mathbf{h}$. Furthermore, the accuracy of the estimates scales well with the number of nodes as it essentially increases the size of the LHS of (65) leading to better estimates.

REFERENCES

[1] A. Mishra and R. T. Rajan, "Relative kinematics estimation using accelerometer measurements," in *Proc. 30th Eur. Signal Process. Conf.*, 2022, pp. 1856–1860.

[2] W. S. Tongerson, "Multidimensional scaling: I theory and method," *Psychometrica*, vol. 17, no. 4, pp. 401–419, 1952.

[3] L. M. Blumenthal, *Theory and Applications of Distance Geometry*. Oxford. U.K.: Clarendon Press., 1953.

[4] J. C. Gower, "Euclidean distance geometry," *Math. Scientist*, vol. 7, pp. 1–14, 1982.

[5] J. C. Gower, *Properties of Euclidean and Non-Euclidean Distances*. Amsterdam, The Netherlands: Elsevier Science Publishing Co., Inc., 1985.

[6] T. L. Hayden, J. L. Wells, W.-M. Liu, and P. Tarazaga, "The cone of distance matrices," *Linear Algebra Appl.*, vol. 144, pp. 153–169, 1990.

[7] T. F. Havel and K. Wüthrich, "An evaluation of the combined use of nuclear magnetic resonance and distance geometry for the determination of protein conformations in solution," *J. Mol. Biol.*, vol. 182, pp. 281–294, 1985.

[8] A. Y. Alfakih, A. Khandani, and H. Wolkowicz, "Solving euclidean distance matrix completion problem via semidefinite programming," *Comput. Optim. Appl.*, vol. 12, pp. 13–30, 1999.

[9] P. Biswas and Y. Ye, "Semidefinite programming for ad-hoc wireless sensor network localization," in *Proc. 3rd Int. Symp. Inf. Process. Sensor Netw.*, 2004, pp. 46–54.

[10] A. Amar, Y. Wang, and G. Leus, "Extending the classical multidimensional scaling algorithm given partial pairwise distance measurements," *IEEE Signal Process. Lett.*, vol. 17, no. 5, pp. 473–476, May 2010.

[11] T. Qu and Z. Cai, "A fast multidimensional scaling algorithm," in *Proc. IEEE Conf. Robot. Biomimetics*, Zhuhai, China, 2015, pp. 2569–2574.

[12] I. Dokmanić, J. Ranieri, and M. Vetterli, "Relax and unfold: Microphone localization with euclidean distance matrices," in *Proc. 23rd Eur. Signal Process. Conf.*, 2015, pp. 265–269.

[13] S. Sand et al., "Swarm exploration and navigation on mars," in *Proc. Int. Conf. Localization*, 2013, pp. 1–6.

[14] A. Cornejo and R. Nagpal, "Distributed range-based relative localization of robot swarms," in *Algorithmic Foundations in Robotics XI*, Berlin, Germany: Springer, 2015, pp. 91–107.

[15] K. Nagatani, H. Ishida, S. Yamanaka, and Y. Tanaka, "Three-dimensional localization and mapping for mobile robot in disaster environments," in *Proc. IEEE/RSJ Int. Conf. Intell. Robots Syst.*, vol. 3, 2003, pp. 3112–3117.

[16] V. Chandrasekhar, W. Seah, Y. Choo, and H. Ee, "Localization in underwater sensor networks: Survey and challenges," in *Proc. 1st ACM Int. Workshop Underwater Networks*, vol. 119, 2006, pp. 33–40.

[17] Y. Li, Y. Wang, W. Yu, and X. Guan, "Multiple autonomous underwater vehicle cooperative localization in anchor-free environments," *IEEE J. Ocean. Eng.*, vol. 44, no. 4, pp. 895–911, Oct. 2019.

[18] R. Rajan et al., "Space-based aperture array for ultra-long wavelength radio astronomy," *Exp. Astron.*, vol. 41, no. 1, pp. 271–306, 2016.

[19] N. Bulusu, J. Heidemann, and D. Estrin, "GPS-less low-cost outdoor localization for very small devices," *IEEE Pers. Commun.*, vol. 7, no. 5, pp. 28–34, Oct. 2000.

[20] Y. Sun, P. Finnerty, and C. Ohta, "BLE-Based outdoor localization with two-ray ground-reflection model using optimization algorithms," *IEEE Access*, vol. 12, pp. 45164–45175, 2024.

[21] J. N. Ash and R. L. Moses, "On the relative and absolute positioning errors in self-localization systems," *IEEE Trans. Signal Process.*, vol. 56, no. 11, pp. 5668–5679, Nov. 2008.

[22] X. Shen, L. Xu, Y. Liu, and Y. Shen, "A theoretical framework for relative localization," *IEEE Trans. Inf. Theory*, vol. 70, no. 1, pp. 732–762, Jan. 2024.

[23] Z. Liu, W. Dai, and M. Z. Win, "Mercury: An infrastructure-free system for network localization and navigation," *IEEE Trans. Mobile Comput.*, vol. 17, no. 5, pp. 1119–1133, May 2018.

[24] J. D. Hol, F. Dijkstra, H. Luinge, and T. B. Schön, "Tightly coupled UWB/IMU pose estimation," in *Proc. IEEE Int. Conf. Ultra-Wideband*, 2009, pp. 688–692.

[25] M. W. Mueller, M. Hamere, and R. D'Andrea, "Fusing ultra-wideband range measurements with accelerometers and rate gyroscopes for quadrocopter state estimation," in *Proc. IEEE Int. Conf. Robot. Automat.*, 2015, pp. 1730–1736.

[26] N. Dwek et al., "Improving the accuracy and robustness of ultra-wideband localization through sensor fusion and outlier detection," *IEEE Robot. Automat. Lett.*, vol. 5, no. 1, pp. 32–39, Jan. 2020.

[27] F. Cakmak, E. Uslu, S. Yavuz, M. F. Amasyali, M. Balcilar, and N. Altuntas, "Using range and inertia sensors for trajectory and pose estimation," in *Proc. 22nd Signal Process. Commun. Appl. Conf.*, 2014, pp. 506–509.

[28] X. Fang, C. Wang, T.-M. Nguyen, and L. Xie, "Graph optimization approach to range-based localization," *IEEE Trans. Syst., Man, Cybern. Syst.*, vol. 51, no. 11, pp. 6830–6841, Nov. 2021.

[29] A. Alcocer, P. Oliveira, A. Pascoal, and J. Xavier, "Estimation of attitude and position from range-only measurements using geometric descent optimization on the special euclidean group," in *Proc. 9th Int. Conf. Inf. Fusion*, 2006, pp. 1–8.

[30] S. Chen and K. C. Ho, "Localization of a mobile rigid sensor network," in *Proc. 24th Eur. Signal Process. Conf.*, 2016, pp. 1368–1372.

[31] S. P. Chepuri, A. Simonetto, G. Leus, and A.-J. van der Veen, "Tracking position and orientation of a mobile rigid body," in *Proc. 5th IEEE Int. Workshop Comput. Adv. Multi-Sensor Adaptive Process.*, 2013, pp. 37–40.

[32] Z. Li, L. Sun, and E. C. Ifeachor, "Range-based relative velocity estimations for networked mobile devices," *IEEE Trans. Veh. Technol.*, vol. 58, no. 4, pp. 2095–2099, May 2009.

[33] D. Moore, J. Leonard, D. Rus, and S. Teller, "Robust distributed network localization with noisy range measurements," in *Proc. Int. Conf. Embedded Networked Sensor Syst.*, 2004, pp. 50–61.

[34] R. T. Rajan, G. Leus, and A.-J. van der Veen, "Relative velocity estimation using multidimensional scaling," in *Proc. 5th IEEE Int. Workshop Comput. Adv. Multi-Sensor Adaptive Process.*, 2013, pp. 125–128.

[35] R. T. Rajan, G. Leus, and A.-J. van der Veen, "Joint relative position and velocity estimation for an anchorless network of mobile nodes," *Signal Process.*, vol. 115, pp. 66–78, 2015.

[36] R. T. Rajan, G. Leus, and A.-J. van der Veen, "Relative kinematics of an anchorless network," *Signal Process.*, vol. 157, pp. 266–279, 2019.

[37] P. Tabaghi, I. Dokmanić, and M. Vetterli, "Kinetic euclidean distance matrices," *IEEE Trans. Signal Process.*, vol. 68, pp. 452–465, 2020.

[38] K.-W. E. Chu, "Symmetric solutions of linear matrix equations by matrix decompositions," *Linear Algebra Appl.*, vol. 119, pp. 35–50, 1989.

[39] I. Borg and P. J. F. Groenen, *Modern Multidimensional Scaling: Theory and Applications*, 2nd ed. Berlin, Germany: Springer Science Business Media, 1998.

[40] M. Kok, J. D. Hol, and T. B. Schön, "Using inertial sensors for position and orientation estimation," *Foundations Trends Signal Process.*, vol. 11, no. 1–2, pp. 1–153, 2017.

[41] D. E. Rutherford, *Classical Mechanics*. Oliver & Boyd, 1957.

[42] K. Hidaka, "Holonomic automated guided vehicle control based on adaptive inverse dynamics control," in *Proc. Int. Conf. Control, Automat. Syst.*, 2008, pp. 2715–2718.

[43] D. Nar and R. Kotecha, "Optimal waypoint assignment for designing drone light show formations," *Results Control Optim.* vol. 9, 2022, Art. no. 100174.

[44] P. Stoica and B. C. Ng, "On the Cramer - Rao bound under parametric constraints," *IEEE Signal Process. Lett.*, vol. 5, no. 7, pp. 177–179, Jul. 1998.

[45] "Bitcraze Datasheet loco positioning deck - REV 1," Accessed: May 17, 2023. [Online.] Available: https://www.bitcraze.io/documentation/hardware/loco_deck/loco_deck-datasheet.pdf,

[46] A. Mishra, "Estimation of relative kinematics parameters of an anchorless network," 2023. [Online.] Available: https://github.com/asil-lab/AM_J1_relative_kinematics

[47] J. J. G. Dúperoux, R. Dinaux, M. Wessendorp, and G. C. H. E. de Croon, "A novel obstacle detection and avoidance dataset for dronest," *Syst. Eng. Constrained Embedded Syst.*, 2022, pp. 8–13, doi: 10.1145/3522784.3522786.

[48] J. Delmerico, T. Cieslewski, H. Rebecq, M. Faessler, and D. Scaramuzza, "Are we ready for autonomous drone racing? The UZH-FPV drone racing dataset," in *Proc. Int. Conf. Robot. Automat.*, 2019, pp. 6713–6719.

[49] J. S. Abel, "A divide and conquer approach to least-squares estimation," *IEEE Trans. Aerosp. Electron. Syst.*, vol. 26, no. 2, pp. 423–427, Mar. 1990.